Lithos 113 (2009) 190–212

Contents lists available at ScienceDirect

Lithos

journal homepage: www.elsevier.com/locate/lithos

Geochemical and Sr–Nd–Pb–O isotopic compositions of the post-collisional ultrapotassic magmatism in SW Tibet: Petrogenesis and implications for India intra-continental subduction beneath southern Tibet

Zhidan Zhao [a,*], Xuanxue Mo [a,*], Yildirim Dilek [b], Yaoling Niu [c], Don J. DePaolo [d], Paul Robinson [e], Dicheng Zhu [a], Chenguang Sun [a], Guochen Dong [a], Su Zhou [a], Zhaohua Luo [a], Zengqian Hou [f]

[a] State Key Laboratory of Geological Processes and Mineral Resources, and School of Earth Science and Mineral Resources, China University of Geosciences, Beijing 100083, China
[b] Department of Geology, Miami University, Oxford, OH 45056,USA
[c] Department of Earth Sciences, Durham University, Durham DH1 3LE, UK
[d] Center for Isotope Geochemistry, University of California, Berkeley, CA 94720, USA
[e] Department of Earth Sciences, Dalhousie University, Halifax, Nova Scotia, Canada B3H 4J1
[f] Institute of Geology, Chinese Academy of Geological Sciences, Beijing 100037, China

ARTICLE INFO

Article history:
Received 2 October 2008
Accepted 13 February 2009
Available online 9 March 2009

Keywords:
Tibetan plateau
Sr–Nd–Pb–O isotopes
Ultrapotassic rocks
India continental subduction

ABSTRACT

Ultrapotassic lavas having distinct geochemical compositions (K_2O/Na_2O >2, K_2O >3%, and MgO >3%) are common and widespread on the Tibet Plateau, where they are closely linked to N–S-trending normal faults. The Tibetan ultrapotassic rocks range in age from ~8 to 24 Ma, slightly older than the spatially associated potassic rocks (10–22 Ma). These lavas consist mainly of trachyte, trachyandesite, basaltic trachyandesite, phonolite and tephriphonolite. They have high light rare earth element (LREE) and large ion lithophile element (LILE) concentrations, but are low in high field strength elements (HFSE). They are characterized by having extremely radiogenic Sr ($^{87}Sr/^{86}Sr_{(i)}$ = 0.710719 to 0.736451) and Pb isotopes ($^{206}Pb/^{204}Pb$ = 18.449–19.345, $^{207}Pb/^{204}Pb$ = 15.717–15.803, $^{208}Pb/^{204}Pb$ = 39.443–40.168) with unradiogenic Nd isotopes ($\varepsilon_{Nd(0)}$ = −7.6 to −15) and old Nd model ages (T_{DM} = 1.3–2.1 Ga), similar in character to the Himalaya crystalline basement. Their isotopic character is interpreted to reflect subduction of the Indian plate beneath the Lhasa terrane, leading to a highly contaminated mantle source. Delamination of the subducted oceanic/continental materials may have played an essential role in the genesis of the ultrapotassic rocks in the Lhasa terrane. The available geological, geochemical and geophysical data favor a model in which the Indian plate was subducted under southern Tibet.

1. Introduction

Northward subduction of the Indian plate beneath Tibet after the India–Asian convergence between about 55 and 65 Ma (Yin and Harrison, 2000) is one of the most interesting aspects of the geological evolution of the Tibetan Plateau, but the geological consequences of this subduction are unclear (Harrison et al., 1992; Yin and Harrison, 2000; Tapponnier et al., 2001; Johnson, 2002). Some tectonic models speculate that the Indian plate was underthrust or injected northward beneath part or all of Tibet, and link this process to the uplift of the plateau (Argand, 1924; Powell and Conaghan, 1973; Barazangi and Ni, 1982; Zhao and Morgan, 1987; Beghoul et al., 1993; Zhou and Murphy, 2005). Other models propose that the Indian plate was not emplaced beneath Tibet, but rather acted as a rigid block moving northward that caused thickening of the plateau (Molnar and Tapponnier, 1975; England and Houseman, 1986; Dewey et al., 1988;) and that led eventually to convective removal of the thickened lithospheric mantle (Houseman et al., 1981; England and Houseman, 1989). Some other models propose inward-dipping subduction (Kosarev et al., 1999; Tapponnier et al., 2001; Kind et al., 2002) or southward-directed subduction and roll-back (Willett and Beaumont, 1994). Recently acquired seismic and gravity data suggest downwelling of the Indian continental plate and its penetration into the deep lithosphere beneath the Bangong–Nujiang suture of central Tibet (Zhao et al., 1993; Jin et al., 1996; Owens and Zandt, 1997; Chen and Ozalaybey, 1998; Kosarev et al., 1999; Chemenda et al., 2000; Tilmann et al., 2003).

The widespread post-collisional magmatism that took place on the Tibetan Plateau from ~60 Ma onward provides a valuable indicator of the composition and nature of the deep lithosphere. It should record the convective thinning of the underlying lithospheric mantle and uplift of the plateau, which strongly impacted the Cenozoic global

* Corresponding authors. Division of Petrology and Mineralogy, School of Earth Science and Mineral Resources, China University of Geosciences, 29 Xue-Yuan Road, Haidian District, Beijing 100083, China.
E-mail addresses: zdzhao@cugb.edu.cn (Z. Zhao), moxx@cugb.edu.cn (X. Mo), dileky@muohio.edu (Y. Dilek).

0024-4937/$ – see front matter © 2009 Elsevier B.V. All rights reserved.
doi:10.1016/j.lithos.2009.02.004

climate (Coulon et al., 1986; Arnund et al., 1992; Turner et al., 1993, 1996; Chung et al., 1998; Miller et al., 1999; Williams et al., 2001; Zhao et al., 2001; Ding et al., 2003; Nomade et al., 2004; Williams et al., 2004; Chung et al., 2005; Mo et al., 2006a; Guo et al., 2006; Gao et al., 2007a).

The Lhasa terrane in southern Tibet is the youngest of several terranes accreted to Asia and the closest to the suture between India and Asia. We have focused on the post-collisional ultrapotassic rocks in this terrane in order to understand their petrogenesis, to evaluate the nature of their source region, and to determine the nature of the relationship between the magmatism and the subduction of the Indian plate. We report new geochemical and isotopic data (Nd, Sr, Pb, and O isotopes) for the ultrapotassic rocks. Our results, together with other published data, show that the lithospheric mantle beneath the central and northern Tibetan Plateau (Qiangtang, Hoh Kil and West Kunlun) is an undisturbed, ancient enriched source region that has not changed since ~60 Ma. On the other hand, the mantle beneath the Lhasa terrane, although geochemically a part of this region, was strongly modified by subduction of Tethyan oceanic lithosphere and the Indian continent, particularly between about 8 and 24 Ma. We propose a two-stage upper mantle delamination model, coupled with subduction of the Indian plate, for the generation of the ultrapotassic, post-collisional magmatism of the Lhasa terrane.

2. Geological setting

2.1. Outline of Lhasa terrane

The Lhasa terrane is located in southern Tibet, between the Neo-Tethyan Bangong–Nujiang suture to the north and the Yarlung Zangbo suture to the south (Fig. 1). The Yarlung Zangbo suture marks the final collision between India and Asia at about 65 Ma (Mo et al., 2003). The southern part of the Lhasa terrane is dominated by the Gangdese batholith of late Cretaceous and early Tertiary age (Mo et al., 2005; Wen et al., 2008) and the Linzizong volcanic rocks, which were erupted between ~65 and 45 Ma (Zhou et al., 2004; Mo et al., 2006a). All of the magmatism is attributed to northward subduction of Tethyan oceanic lithosphere (Mo et al., 2007, 2008). Similar Andean-type, arc-related volcanic and intrusive rocks with Mesozoic ages are widely distributed in the middle and northern parts of the Lhasa terrane, where they are related to earlier subduction that formed the Bangong–Nujiang suture (Zhu et al., 2006).

Both the sedimentary strata and magmatic rocks in the Lhasa terrane trend east–west, roughly parallel to the Yarlung Zangbo suture. Paleozoic to Paleogene sedimentary rocks crop out in the central part of the terrane where they are associated with volcanic rocks (Yin and Harrison, 2000), such as the Jurassic–Cretaceous Yeba Formation and the Sangri Group (Zhu et al., 2008a,b). The Amdo amphibolite facies orthogneiss near the Bangong–Nujiang suture is the oldest crystalline basement known in the Lhasa terrane (852 Ma; Guynn et al., 2006). Intra-plate magmatism in the Lhasa terrane postdating the Asia–India collision is represented by ore-bearing adakites (18–12 Ma; Chung et al., 2003; Hou et al., 2004; Guo et al., 2007; Gao et al., 2007b), and potassic and ultrapotassic volcanic rocks (~24–8 Ma; Chung et al., 2005; Mo et al., 2006a). These volcanic rocks have been studied extensively over the last decade and have yielded important information on the Cenozoic evolution of the Tibetan Plateau.

2.2. General features of postcollisional potassic and ultrapotassic rocks in the Lhasa terrane

The definition of "ultrapotassic rocks" introduced by Foley et al. (1987) is based on their whole-rock chemistry other than mineralogy. The ultrapotassic rocks (K_2O/Na_2O >2, K_2O >3%, and MgO >3%) can be further divided into three sub-groups (I—lamproites, II—kamafugites and III—other rocks that occur in orogenic areas). Most of these rocks contain not only olivine, but also K-rich minerals, such as leucite and phlogopite. Commonly, ultrapotassic rocks are associated with large or super-large Cu–Au deposits (Müller and Groves, 2000).

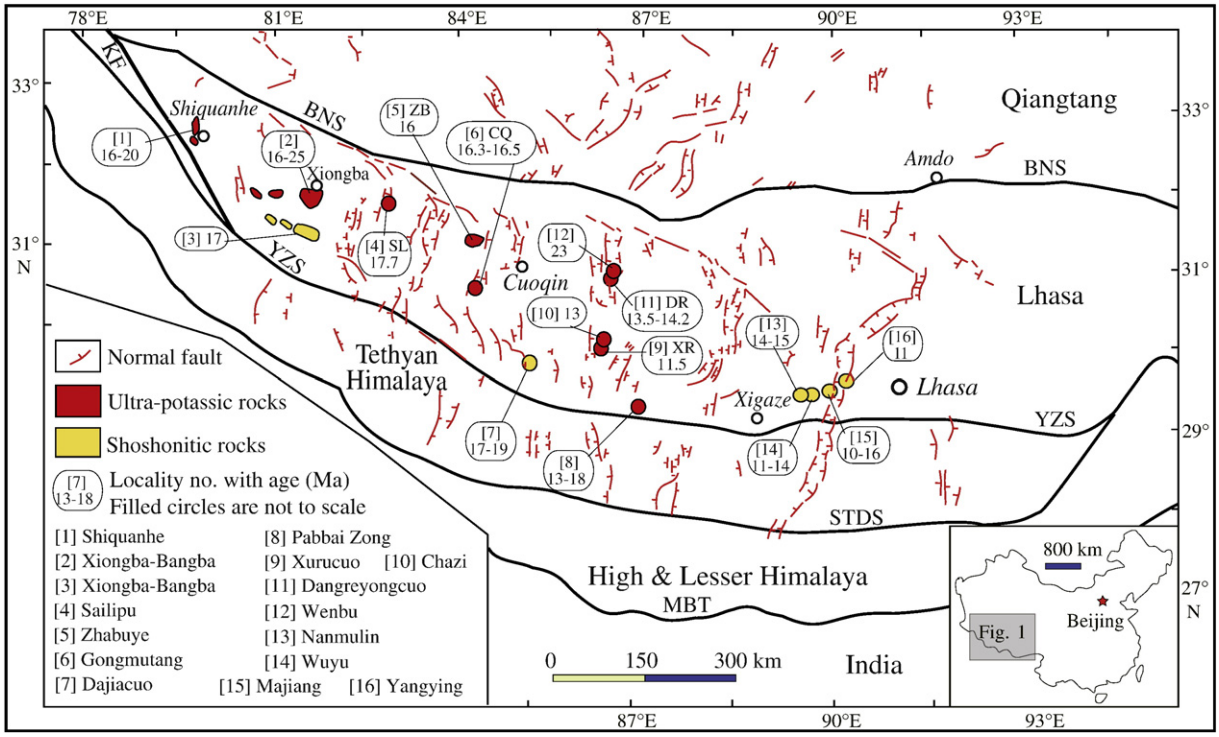

Fig. 1. Distribution of post-collisional shoshonitic and ultrapotassic volcanic rocks in the Lhasa terrane, southern Tibet (modified from Zhao et al., 2006). See Table 1 for descriptions of locality, rock type, age and data sources with the same field number for the rocks. North–south trending normal faults are after Blisniuk et al. (2001). MBT = Main Boundary Thrust; STDS = South Tibet Detachment System; YZS = Yarlung Zangbo Suture; KF = Karakorum Fault; BNS = Bangong–Nujiang Suture.

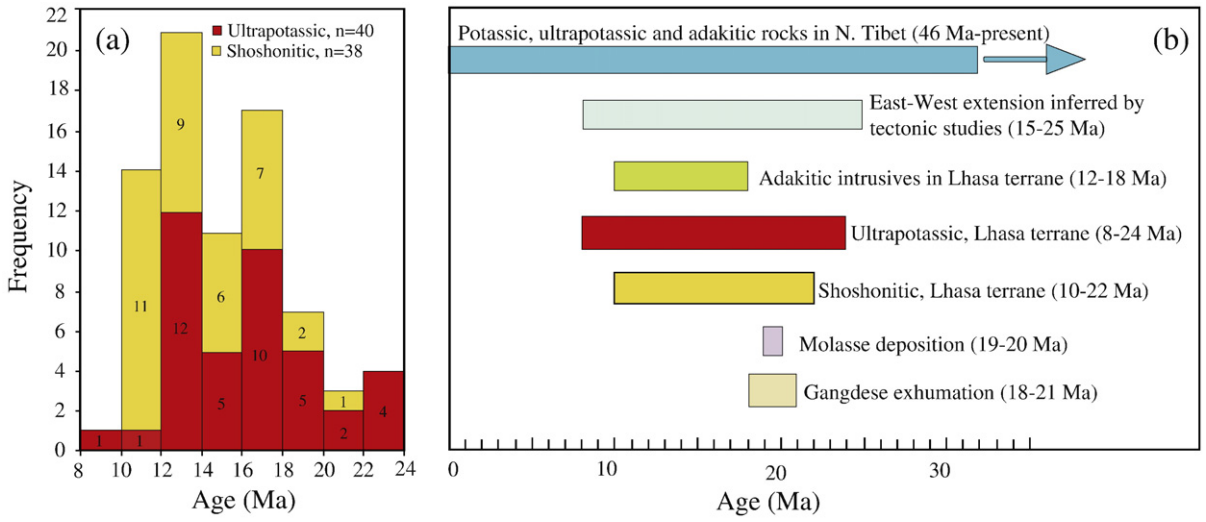

Fig. 2. (a) Histogram showing ages of the ultrapotassic and shoshonitic rocks in the Lhasa terrane; (b) Age span of the post-collisional magmatism and tectonic events in the Lhasa terrane and adjacent areas. Data sources in (a) are as in Table 1. Data sources in (b) are: Shoshonitic, ultrapotassic, and adakitic rocks in N. Tibet from Chung et al. (2005)), Wang et al. (2005, 2008a,b), Williams et al. (2004), Guo et al. (2006), Deng (1998), Ding et al. (2003), Turner et al. (1996), East–west extension time span and molasse deposition from Harrison et al. (1992), Coleman and Hodges (1995), Blisniuk et al. (2001), Pêcher et al. (1991), Adakitic rocks from Chung et al. (2003), Hou et al. (2004), Gao et al. (2007a), Gangdese batholith exhumation from Copeland et al. (1987).

Ultrapotassic rocks range in age from Precambrian to the present (Corriveau, 1990; Da Silva Filho et al., 1993). The youngest potassic and ultrapotassic rocks (<60 Ma) typically occur in five tectonic settings; continental arc, post-collisional arc, initial oceanic arc, late oceanic arc, and within-plate settings. All of these environments, except for within-plate settings, are closely related to subduction zones.

Most commonly, these rocks occur in continental arc settings, such as those of the Andean volcanic belt, the North American Cordillera, the Roman Province and the Aeolian Islands. Typical post-collisional arcs occur in the Alps, Anatolia, and Iran, which collectively mark areas of young orogenic belts associated with continental collision (Müller and Groves, 2000; Dilek and Altunkaynak, 2007, 2008). The ultrapotassic magmatism in southern Tibet must have taken place in a post-collisional arc tectonic setting, shortly after subduction of Tethyan oceanic lithosphere and the collision between India and Asia.

Previous works on post-collisional shoshonitic and ultrapotassic volcanic magmatism have focused mostly on the northern and eastern parts of the Tibetan Plateau (e.g. Arnund et al., 1992; Turner et al., 1993, 1996; Chung et al., 1998; Deng, 1998; Wang et al., 2001a,b, Xu et al., 2001), and very limited data were available on such rocks in the Lhasa terrane (Coulon et al., 1986; Turner et al., 1996) until new outcrops were found as part of a geological mapping project (scale 1:250,000) sponsored by the China Geological Survey in 2000. The volumes of potassic and ultrapotassic volcanic rocks in the Lhasa

Table 1
Summary of published ages of potassic and ultrapotassic volcanic rocks in the Lhasa terrane, Tibet.

Field no.	Locality	Rock type	Method	Mineral/whole rock	Age (Ma)	Sample numbers	Data source
[1]	Shiquanhe	Trachyte, rhyolite	Ar–Ar	Minerals	16–20	3	Turner et al. (1996)
[1]	Shiquanhe	Trachyandesite	Ar–Ar	Phlogopite	21.2–24	3	Williams et al. (2004)
[2]	Xungba–Bangba	Potassic and ultrapotassic	Ar–Ar, Rb–Sr	Minerals and whole rock	18–23	6	Miller et al. (1999)
[3]	Xungba–Bangba	Calc-alcline	Ar–Ar, Rb–Sr	Minerals and whole rock	16–17	11	Miller et al. (1999)
[4]	Sailipu basin	Trachyandesite	U–Pb	Zircon	17.7	1	Sun et al. (2008)
[4]	Sailipu basin	Trachyandesite	Ar–Ar	Phlogopite	17.6	1	Wang et al. (2008a,b)
[5]	Zabuye salt lake	Trachyandesite	Ar–Ar	Sanidine and biotite	16.07–16.23	6	Nomade et al. (2004)
[5]	Zabuye salt lake	Trachyandesite	K–Ar	Whole rock	15.8–15.9	2	Ma et al. (2002)
[5]	Zabuye salt lake	Trachyandesite	Ar–Ar	Whole rock	15.53	1	Chen et al. (2006)
[6]	Gongmutang, Zhongba	Trachyandesite	Ar–Ar	Whole rock	16.3–16.5	2	Mo et al. (2006a,b)
[6]	Gongmutang, Zhongba	Trachyandesite	Ar–Ar	Phlogopite	17.4	2	Ding et al. (2006)
[7]	Dajiacuo, Angren	Dacite	Ar–Ar	Amphinolite and whole rock	17–19	2	Williams et al. (2001)
[7]	Dajiacuo, Angren	Trachyte	Ar–Ar	Phlogopite	18.8	1	Williams et al. (2004)
[8]	Pabbai Zong	Ultrapotassic rocks	Ar–Ar	Phlogopite	13–18	4	Williams et al. (2001)
[9]	Xurucuo, Angren	Trachyte	Ar–Ar	Phlogopite	11.2	1	Zhao et al. (2006)
[10]	Chazi, Angren	Trachyte, trachyandesite	Ar–Ar	Phlogopite	8.2–13.3	3	Ding et al. (2003)
[11	Dangreyong lake, Nima	Trachyte	Ar–Ar	Phlogopite and sanidine	13.0–13.7	4	Zhao et al. (2006)
[11]	Dangreyong lake, Nima	Ultrapotassic, leucite phonolite	K–Ar	Whole rock	12.6	1	Liao et al. (2002)
[11]	Dangreyong lake, Nima	Trachyandesite	Ar–Ar	Phlogopite	13.5	1	Ding et al. (2006)
[12]	Wenbu, Nima	Trachyte and phonolite	Ar–Ar	Sanidine	23	2	Ding et al. (2003)
[13]	Nanmulin	Dacite	Ar–Ar	Sanidine and phlogopite	14.03–15.10	4	Spicer et al. (2003)
[13]	Nanmulin	Andesite, dacite, and rhyolite	Ar–Ar	Biotite	12.5–13.9	3	Williams et al. (2004)
[14]	Wuyu basin, Nanmulin	Trachyte, trachyandesite	Ar–Ar	Sanidine and biotite	12.00–13.63	5	Zhou (2002)
[14]	Wuyu basin, Nanmulin	Granite porphyry	Ar–Ar	Sanidine	10.84	1	Zhou (2002)
[15]	Majiang, Nimu	Andesite, trachyte	Ar–Ar	Sanidine, Plagioclase, etc	10–16	5	Coulon et al. (1986)
[16]	Yangying, Dangxiong	Rhyolite	Ar–Ar	Sanidine and biotite	10.65–10.92	3	Nomade et al. (2004)

Field numbers are as those shown in Fig. 1.

terrane are much greater than previously thought (Miller et al., 1999; Zhao et al., 2000, 2001; Williams et al., 2001; Ma et al., 2002; Liao et al., 2002; Zhao et al., 2003a,b; Spicer et al., 2003; Ding et al., 2003; Williams et al., 2004; Nomade et al., 2004; Chung et al., 2005; Chen et al., 2006; Ding et al., 2006; Mo et al., 2006a; Zhao et al., 2006; Gao et al., 2007a) and these rocks have helped to delineate the tectonic processes involved in the formation of the plateau as proposed by Harrison et al. (1992).

A summary of the studies of the potassic and ultrapotassic lavas of the Lhasa terrane listed above shows that: (1) They are closely related to N–S-trending normal faults (also called N–S rifts, graben or the east–west extensional tectonics), and to N–S elongated lakes and Cenozoic basins. In contrast to the Gangdese batholith, which trends east–west parallel to the Yarlung Zangbo suture, the potassic and ultrapotassic lavas are scattered irregularly along the Yarlung Zangbo suture in southern Tibet, and along the Bangong–Nujiang suture farther north. (2) The ultrapotassic lavas crop out only west of longitude 87°E, whereas the potassic lavas crop out between Shiquanhe and Lhasa, and are not limited geographically. This suggests some systematic differences between the western and eastern parts of the Lhasa terrane (Hou et al., 2006). (3) The ultrapotassic rocks range in age from 24 to 8 Ma, spanning a longer period of time than the potassic rocks (22–10 Ma; Fig. 2a). In addition, the ultrapotassic rocks become younger from west to east (Table 1). The eruption of both the potassic and ultrapotassic rocks overlaps other tectono-magmatic events in the region, e.g. E–W extension, exhumation of the Gangdese batholith, intrusion of adakitic porphyries and deposition of molasse sediments, suggesting that they may all be linked to deep lithospheric processes (Williams et al., 2004; Hou et al., 2004; Zhao et al., 2006). (4) The K-rich rocks are mainly trachyte, trachyandesite, basaltic trachyandesite, phonolite and tephriphonolite, showing typical ultrapotassic and shoshonitic geochemistry. (5) All of the rocks, but especially the ultrapotassic varieties, are extremely enriched in LREE and LILE and depleted in HFSE. They also have extremely high Sr and Pb and low Nd isotopic values, similar to those of the Himalayan basement. This supports the interpretation that subduction of the Indian plate beneath Lhasa terrane affected the source region of these rocks (Zhao et al., 2003a,b; Ding et al., 2003; Mo et al., 2006a,b). (6) Although a number of models have been proposed to explain the origin of the ultrapotassic rocks, all of them invoke low degrees of melting of a metasomatised upper mantle. Such an origin is supported by the composition of mantle xenoliths in ultrapotassic rocks from Sailipu basin in western Lhasa terrane (Zhao et al., 2008a,b).

3. Petrography

Our samples were collected across the Lhasa terrane, from west to east, at Sailipu basin, Zabuye salt lake, Gongmutang, Dangreyong lake,

Table 2
Phenocryst and groundmass mineral assemblages of the ultrapotassic volcanic rocks in Lhasa terrane, Tibet.

Sample	Locality	Field no.	Age (Ma)	Mg-no	Rock type	Phenocrysts (vol.%)	Groundmass
CQ01	Gongmutang	6	16.1	0.76	S2	Ol(15)	Cpx + Sa + Fe–Ti
CQ02	Gongmutang	6	16.59	0.56	S3	Ol(20)	Cpx + Ol + Pl + Sa + Fe–Ti
CQ03	Gongmutang	6		0.74	S2	Ol(10)	Cpx + Ol + Pl + Sa + Fe–Ti
D9103	Gongmutang	6		0.62	S3	Phl(20) + Cpx(5) + Ol(5)	Sa + Fe–Ti
GGP-7	Gongmutang	6		0.76	U1	Ol(15) + Cpx(8)	Cpx + Ol + Fe–Ti
XR01-1	Xuru lake	9		0.59	T	Cpx(10) + Phl(8) + Sa(6) + Ne(5) + Pl(1)	Cpx + Sa + Fe–Ti
XR01-3	Xuru lake	9	11.5	0.76	S2	Cpx(23) + Phl(12)	Sa + Cpx + Fe–Ti
XR02-1	Xuru lake	9		0.68	U3	Phl(35)	Cpx + Sa
DR01-1	Dangreyong lake	11	13.4	0.56	T	Sa(15) + Cpx(8) + Ap(2)	Sa + Cpx + Fe–Ti
DR01-2	Dangreyong lake	11	13.7	0.58	T	Sa(15) + Cpx(8) + Ap(2)	Sa + Cpx + Fe–Ti
DR03	Dangreyong lake	11	14.2	0.56	T	Sa(23) + Phl(15) + Cpx(5) + Ap(2)	Sa + Cpx + Fe–Ti
DR04	Dangreyong lake	11	13.5	0.57	T	Sa(20) + Phl(10) + Cpx(15) + Ap(2)	Sa + Cpx + Fe–Ti
Z8030-5	Dangreyong lake	11	13.47	0.65	T	Cpx(5) + Phl(8)	Cpx + Phl + Lct + Fe–Ti + Glass
Z8030-18	Dangreyong lake	11	13.17	0.61	S3	Sa(6) + Cpx(7) + Phl(9)	Sa + Cpx + Lct + Ap + Fe–Ti
ZB1	Zabuye salt lake	5	16.16	0.56	S3	Cpx(2) + Sa(3) + Phl(1)	Cpx + Sa + Phl + Ap + Fe–Ti
ZB3	Zabuye salt lake	5		0.60	S3	Cpx(5) + Sa(4) + Phl(1) + Ol	Cpx + Sa + Phl + Fe–Ti
ZB4	Zabuye salt lake	5	16.12	0.57	S3	Cpx(6) + Sa(4) + Phl(1)	Cpx + Sa + Phl + Fe–Ti
ZB6	Zabuye salt lake	5		0.60	S3	Cpx(7) + Sa(6) + Phl(1) + Ol	Cpx + Sa + Phl + Fe–Ti
ZB8	Zabuye salt lake	5		0.60	S3	Cpx(7) + Sa(8) + Phl(1) + Ol	Cpx + Sa + Phl + Fe–Ti
ZB9	Zabuye salt lake	5		0.60	S3	Cpx(8) + Sa(8) + Phl(1) + Ol	Cpx + Sa + Phl + Fe–Ti + G
ZB10	Zabuye salt lake	5	16.1	0.57	S3	Cpx(3) + Sa(4) + Phl(2)	Cpx + Sa + Phl + Fe–Ti + G
ZB11	Zabuye salt lake	5		0.60	S3	Cpx(3) + Sa(3) + Phl(2) + Ol	Cpx + Sa + Phl + Fe–Ti + G
ZB12	Zabuye salt lake	5	16.1	0.57	S3	Cpx(2) + Sa(1) + Phl(1) + Ol	Cpx + Sa + Phl + Fe–Ti + G
ZB14	Zabuye salt lake	5		0.56	S3	Cpx(3) + Sa(1) + Phl(1) + Ol	Cpx + Sa + Phl + Fe–Ti + G
ZB16	Zabuye salt lake	5		0.58	S3	Cpx(3) + Sa(2) + Phl(2)	Cpx + Sa + Phl + Fe–Ti + G
ZB18	Zabuye salt lake	5		0.58	S3	Cpx(3) + Sa(3) + Phl(1)	Cpx + Sa + Phl + Fe–Ti + G
ZB20	Zabuye salt lake	5		0.58	S3	Cpx(3) + Sa(4) + Phl(1)	Cpx + Sa + Phl + Fe–Ti + G
SL0618*	Sailipu basin	4		0.66	S3	Cpx + Ol	Sa + Cpx + Fe–Ti + G
SL0619*	Sailipu basin	4		0.65	S3	Phl(2) + Cpx(2)	Sa + Cpx + Phl + Fe–Ti
SL0620*	Sailipu basin	4		0.66	S3	Phl(1) + Cpx(1) + Ol	Sa + Cpx + Phl + Fe–Ti
SL0621*	Sailipu basin	4		0.72	S3	Ol(2) + Cpx(1)	Sa + Cpx + Fe–Ti + G
SL0622*	Sailipu basin	4		0.64	S3	Ol(1) + Cpx(1)	Sa + Cpx + Fe–Ti + G
SL0623*	Sailipu basin	4		0.73	S3	Ol(1) + Cpx(1)	Sa + Cpx + Phl + Fe–Ti
SL0624*	Sailipu basin	4		0.74	S3	Ol(1) + Cpx(2) + Phl(1)	Sa + Cpx + Phl + Fe–Ti
SL0625*	Sailipu basin	4		0.65	S3	Ol(1) + Cpx(2) + Phl(1)	Sa + Cpx + Phl + Fe–Ti
SL0628*	Sailipu basin	4	17.7	0.59	S3	Cpx(3) + Phl(1)	Sa + Cpx + Phl + Fe–Ti
SL0630*	Sailipu basin	4		0.74	S3	Ol + Cpx + Phl	Sa + Cpx + Phl + Fe–Ti
SL0631*	Sailipu basin	4		0.69	S3	Ol(2) + Cpx(1) + Phl(1)	Sa + Cpx + Opx + Phl + Fe–Ti

Field number refers to number of the volcanic field outcrops in Fig. 1. Ages are from Table 1. Rock type is determined by Fig. 3a.
Names shown by letters are as follows: S1, trachybasalt; S2, basaltic trachyandesite; S3, trachyandesite; T, trachyte; U1, tephrite; U2, phonotephrite; U3, tephriphonolite; Ap, apatite; Cpx, clinopyroxene; Fe–Ti, Fe–Ti oxides; G, glass; Lct, leucite; Ne, nepheline; Ol, olivine; Opx, orthopyroxene; Ph, phlogopite; Pl, plagioclase; Sa, sanidine. Proportions in percent of phenocrysts are shown in parentheses (vol.%). *Samples in Sailipu contain mantle xenoliths.

and Xuru lake (Fig. 1). All the rocks have ^{40}Ar–^{39}Ar or zircon LA-ICPMS ages between 11.5 and 17.7 Ma (Nomade et al., 2004; Mo et al., 2006a, b; Zhao et al., 2006; Sun et al., 2008; Table 1). Descriptions of the localities, rock types, and petrography of the samples are given in Table 2. All of the ultrapotassic volcanic rocks studied are porphyritic with 1 to 47 modal % phenocrysts. Relatively mafic samples from Gongmutang, Sailipu, and Zabuye generally contain <20 modal% phenocrysts, mainly olivine, clinopyroxene, phlogopite and sanidine, set in a groundmass of the same minerals plus apatite, Fe–Ti oxides and glass. More felsic samples from Xuru and Dangreyong lakes are highly phyric with up to 47 modal % phenocrysts, chiefly clinopyroxene, sanidine and phlogopite with little or no olivine. The groundmass of these rocks commonly contains both nepheline and leucite (Table 2).

4. Analytical methods

4.1. Mineral analyses

The mineral assemblages and textures of 38 samples of ultrapotassic volcanic rocks in Lhasa terrane were obtained by petrographic analysis (Table 2). Major element compositions of representative minerals were analyzed on a JEOL Superprobe JXA 8100 at the Institute of Geology and Geophysics, Chinese Academy of Sciences (IGCAS), China, using an accelerating voltage of 15 kV, beam current of 1×10^{-8} A and spot diameter of 1 μm. Calibration of elemental analyses was done using mineral standards from the SPI company (USA) (e.g., SPI 21 diopside for Ca and synthetic Ni_2S for Ni).

4.2. Major and trace elements

Whole-rock geochemical compositions were measured at the State Key Laboratory of Continental Dynamics, Northwest University, Xi'an, China. Major element compositions were determined by XRF (Rikagu RIX 2100) using fused glass disks, whereas trace element compositions were determined by ICP-MS (Elan 6100 DRC) after acid digestion of samples in high-pressure Teflon bombs. Selected trace elements were also analyzed by XRF using pressed-powder pellets. The concentrations of Sr, Y, Nb, Zr, Cr and Ni obtained using these two methods for the same samples generally agree within 10% uncertainty (Rudnick et al., 2004). Analyses of rock standards (AGV-1, GSR-01, and BCR-2) indicate precision and accuracy better than 5% for major elements and 10% for trace and rare earth elements. See Gao et al. (2008) for details.

4.3. Sr and Nd isotopes

Samples were cut into ~1 cm chips from the least-altered interior portions of samples. They were cleaned ultrasonically in ultrapure water for 15 min to wash out the dust. Then they were crushed into smaller pieces of ~2–3 mm, which were cleaned again by ultrapure water and 0.1 N HNO_3 in an ultrasonic bath for 15 min. After the samples were dried, any altered or weathered pieces or steel fragments were picked out under a microscope. In each step, the cleaning procedure was repeated. The cleaned sample pieces were then ground in an agate mortar to pass a ~200 mesh. Both the agate mortar and pestle were cleaned with high purity clean sand (SiO_2) powder and 6 N pure HCl in an ultrasonic bath for 15 min, and then rinsed with ultrapure water. This process was repeated prior to grinding each sample in order to prevent contamination between samples.

The powdered samples were dissolved and analyzed for isotopic ratios of Sr and Nd and isotope-dilution abundances of Rb, Sr, Sm, and Nd. All of the sample preparation and analyses, except for the samples from Sailipu, were carried out in the Center for Isotope Geochemistry at the University of California, Berkeley. Measurements were made on a VG354 mass spectrometer. Details of the analytical procedures are given in DePaolo and Daley (2000). Analyses of NBS-987 standard run during the same

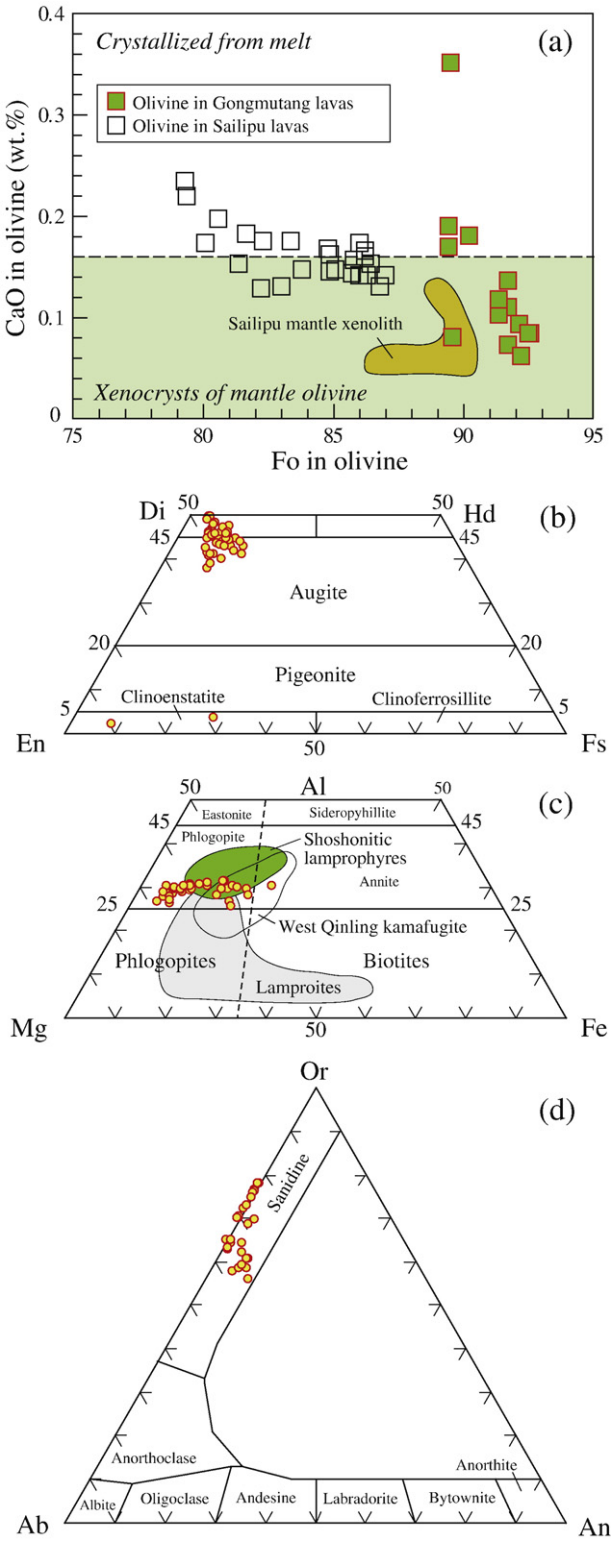

Fig. 3. Phenocryst composition of the ultrapotassic rocks from the Lhasa terrane. (a) Fo (forsterite = 100 Mg/(Mg + Fe), where Mg and Fe represent molar proportions) vs. wt.% CaO plot of olivine phenocrysts, after Thompson and Gibson (2000); (b) Pyroxenes on the enstatite–ferrosilite–diopside–hedenbergite quadrilateral after Morimoto (1988); (c) Micas plotted on the Al–Mg–Fe diagram with lamproites and shoshonitic lamprophyres after Sheppard and Taylor (1992), West Qinling kamafugites data from Yu (1994); (d) Feldspar ternary diagram after Smith (1974).

period gave $^{87}Sr/^{86}Sr = 0.710280 \pm 4$ ($N = 10$). The $^{87}Sr/^{86}Sr$ values are normalized to $^{86}Sr/^{88}Sr = 0.1194$ to correct for mass discrimination. Nd standard AMES was measured as $^{143}Nd/^{144}Nd = 0.510975 \pm 6$ ($N = 5$) during the same running period. For $^{143}Nd/^{144}Nd$, the correction for mass discrimination was done assuming $^{146}Nd/^{142}Nd = 0.636151$. ε_{Nd} is calculated relative to $^{143}Nd/^{144}Nd_{(CHUR)} = 0.511836$:

$$\varepsilon_{Nd} = 10^4\left[\frac{^{143}Nd/^{144}Nd_{sample}}{^{143}Nd/^{144}Nd_{CHUR}} - 1\right].$$

Analytical uncertainty in ε_{Nd} is ± 0.1.

Nd model ages relative to the depleted mantle (T_{DM}) were calculated from:

$$T_{DM} = \frac{1}{\lambda_{Sm}} ln\left[1 + \frac{^{143}Nd/^{144}Nd_{sample} - {}^{143}Nd/^{144}Nd_{DM}}{^{147}Sm/^{144}Nd_{sample} - {}^{147}Sm/^{144}Nd_{DM}}\right]$$

where the decay constant $\lambda_{Sm} = 6.54 \times 10^{-12}$ yr^{-1}, $^{143}Nd/^{144}Nd_{DM} = 0.51235$, and $^{147}Sm/^{144}Nd_{DM} = 0.225$.

The samples from Sailipu basin were dissolved and analyzed at the State Key Laboratory of Geological Processes and Mineral Resources, China University of Geosciences at Wuhan. Measurements were made on a Triton mass spectrometer. The measured $^{143}Nd/^{144}Nd$ and $^{87}Sr/^{86}Sr$ ratios were normalized to $^{146}Nd/^{144}Nd = 0.7219$ and $^{86}Sr/^{88}Sr = 0.1194$ to correct for mass discrimination. Analyses of NBS-987 standard run during the same period gave $^{87}Sr/^{86}Sr = 0.710278 \pm 3$ ($N = 6$). Measurement of the La Jolla Nd standard yielded $^{143}Nd/^{144}Nd = 0.511847 \pm 1$ ($N = 6$) during the same running period. ε_{Nd} and T_{DM} were calculated using the same equations shown above but different parameters were applied. ε_{Nd} was calculated relative to $^{143}Nd/^{144}Nd_{(CHUR)} = 0.512638$. In the T_{DM} calculation, $^{143}Nd/^{144}Nd_{DM} = 0.51315$, and $^{147}Sm/^{144}Nd_{DM} = 0.21357$.

The $^{147}Sm/^{144}Nd$ ratios for the Zabuye samples are from measured isotope-dilution abundances of Sm and Nd, obtained in U. C. Berkeley. The $^{147}Sm/^{144}Nd$ ratios for other samples are calculated from the Sm and Nd contents measured by ICP-MS (Table 7).

4.4. Pb isotopes

All whole-rock Pb analyses including chemical separation and mass spectrometry were performed at the Institute for Geology, Chinese Academy of Science (IGCAS). About 150 mg of rock powder was dissolved with a mixed acid (HF:$HClO_4$ = 10:1) in Teflon vessels. Samples were separated by anion exchange column chemistry using an HBr medium. Isotopic ratios were measured on a VG-354 mass spectrometer, in peak jumping mode. The Pb isotopic ratios were corrected for instrumental fractionation using average measured values of the NBS981 standard. The measured isotopic ratios of the NBS981 showed mass fractionation around 0.1%/amu relative to the recommended values. Total blank levels were less than 1 ng. The results measured for NBS981 are ($\pm 2\sigma$) 0.059135 ($\pm 0.021\%$) for $^{204}Pb/^{206}Pb$, 0.914174 ($\pm 0.010\%$) for $^{207}Pb/^{206}Pb$, and 2.161430 ($\pm 0.016\%$) for $^{208}Pb/^{206}Pb$.

4.5. O isotopes

Oxygen isotope analyses on whole-rock samples and separated minerals were performed in two groups. The first group of samples from Zabuye salt lake was analyzed in the Center for Isotope Geochemistry at The Lawrence Berkeley National Laboratory. Oxygen isotope ratios were measured according to the BrF5 procedure of Clayton and Mayeda (1963). Measurements were made on a Prism Series II Isotope Ratio Mass Spectrometer (IRMS) and are precise to ± 0.2/million. Repeat measurements were identical within the analytical precision. All fractionations and ^{18}O values are reported in units of per million and given relative to the V-SMOW standard. In each extraction run, two samples of the quartz standard NBS-28 ($^{18}O = 9.6$) were included to check for consistency and for data correction within each set of extractions. Oxygen isotope analyses of the other samples were carried out in the Institute of Mineral Resources, Chinese Academy of Geological Sciences, Beijing, using the same BrF5 procedure and a MAT 251 EM Mass Spectrometer. The precision and accuracy are better than ± 0.2/million.

5. Results

5.1. Mineral chemistry

Representative major element compositions of olivine, clinopyroxene, phlogopite, and sanidine are given in Supplementary Tables 3–6, respectively.

Olivine phenocrysts from Gongmutang are undeformed, have high Fo (90–93), low NiO (0.04–0.18 wt.%) and variable CaO (0.06–0.35 wt.%). The grains with low CaO (<0.16 wt.%) are interpreted as mantle xenoliths, whereas those with higher CaO (0.16–0.35 wt.%) probably crystallized from the ultrapotassic magmas (Fig. 3a; Thompson and Gibson, 2000). A zoned olivine shows decreasing MgO and NiO, and increasing CaO from core (Fo_{92}, NiO 0.13 wt.%, CaO 0.06 wt.%) to rim (Fo_{90}, NiO 0.06 wt.%, CaO 0.19 wt.%). Olivine phenocrysts from Sailipu have lower Fo (79–87) and higher NiO (0.20–0.73 wt.%), with CaO ranging from 0.13 to 0.23 wt.%. The Sailipu rocks, like those from Gongmutang, contain both magmatic phenocrysts and mantle xenoliths (Fig. 3a) (Zhao et al., 2008a). Although, xenocrystic olivine, similar to that described by Miller et al. (1999), is present in both samples, we have not recognized significant kink banding, a typical feature of many xenocrysts.

The clinopyroxene phenocrysts are diopside ($Wo_{45-50}En_{43-48}Fs_{4-10}$) and augite ($Wo_{38-45}En_{43-52}Fs_{7-16}$) with high Al_2O_3/TiO_2 ratios (1.7–6.5) and high Mg-numbers (81–96), suggesting that they crystallized under high pressures during magma ascent (Fig. 3b). Orthopyroxene is extremely rare in these rocks; only two crystals of clinoenstatite ($Wo_{1.8}En_{89.5}Fs_{8.7}$ and $Wo_{3.0}En_{68.4}Fs_{28.6}$) were found in samples from Sailipu and Zabuye, respectively.

Phlogopite phenocrysts are very common in all the Tibetan ultrapotassic rocks and are probably mainly responsible for their high bulk-rock K_2O contents (Fig. 3c). Both high-Ti and low-Ti varieties of phlogopite occur randomly in the rocks. Phenocrysts in the low-Ti group (TiO_2 = 1.6–4.7 wt.%) have high Mg-numbers (68–92) and high K_2O (8.6–10.4 wt.%), whereas those in the high-Ti group (TiO_2 = 5–9 wt.%) have relatively low Mg-numbers (62–80) and slightly lower K_2O (8.6–9.6 wt.%). One zoned phlogopite phenocryst has a rim with a higher Mg-number than the core. The phlogopites analyzed in this study are compositionally similar to those in shoshonitic lamprophyres from Australia (Sheppard and Taylor, 1992) and in kamafugites of West Qinling, China (Yu, 1994).

Sanidine is another common K-rich (K_2O = 7–13 wt.%) phase that occurs both as phenocrysts and in the groundmass of the Tibet ultrapotassic rocks. The analyzed grains have compositions in the range of $Or_{56-78}Ab_{22-37}An_{0-9}$ (Fig. 3d).

5.2. Whole-rock major, trace element and Sr–Nd–Pb–O isotope geochemistry

Major oxides, trace elements and Sr–Nd–Pb–O isotopic compositions of the analyzed rocks are listed in Table 7. Most of the lavas analyzed (35 of 40 samples), are typical ultrapotassic rocks according to the geochemical criteria of Foley et al. (1987) (SiO_2 = 45–61 wt.%, $Fe_2O_{3(t)}$ = 4.5–8 wt.%, MgO = 3.8–12.3 wt.%, TiO_2 = 0.8–1.6 wt.%, K_2O = 4.7–8 wt.%, K_2O/Na_2O = 2–4.4). The other five samples, four from Dangreyong lake and one from Sailipu, do not strictly match the geochemical criteria, but are very close in composition to the other

Table 7
Geochemical data of ultrapotassic rocks from the Lhasa terrane, southern Tibet.

Sample	CQ01	CQ02	CQ03	D9103	GGP-7	XR01-1	XR01-3	XR02-1	DR01-1	DR01-2
Locality	Gongmutang	Gongmutang	Gongmutang	Gongmutang	Gongmutang	Xuru lake	Xuru lake	Xuru lake	Dangreyong	Dangreyong
Longtitude	E84°26.3′	E84°26.4′	E84°26.4′	E84°26′	E84°26′	E86°30.8′	E86°30.8′	E86°31.6′	E86°23.5′	E86°23.5′
Latitude	N30°48.9′	N30°48.9′	N30°49.0′	N30°48′	N30°48′	N30°4.3′	N30°4.3′	N30°2.4′	N30°56.6′	N30°56.6′
Altitude (m)	4816	4790	4787			4971	4971	4926	4751	4751
Age (Ma)	16.10 ± 0.12	16.59 ± 0.13					11.5 ± 0.2		13.4 ± 0.2	13.7 ± 0.2
(wt.%)										
SiO_2	51.79	55.80	51.48	56.07	45.39	59.40	52.22	52.47	61.62	59.08
TiO_2	1.42	1.32	1.56	1.35	0.83	0.99	1.41	1.51	0.88	0.93
Al_2O_3	11.41	14.86	11.53	14.25	10.34	13.76	11.51	12.76	14.13	13.55
TFe_2O_3	6.82	6.55	7.11	6.15	7.88	5.23	6.99	6.07	3.90	4.19
FeO	4.08	3.08	4.52	0.20	2.75	0.80	3.95	2.88	1.20	1.58
MnO	0.10	0.11	0.11	0.09	0.13	0.08	0.11	0.10	0.06	0.07
MgO	10.92	4.29	9.96	4.99	12.30	3.81	10.99	6.42	2.50	2.91
CaO	5.92	5.95	6.03	4.84	10.09	4.68	6.06	6.17	2.79	3.72
Na_2O	1.91	2.75	1.48	2.72	1.42	3.11	2.04	1.87	2.69	2.71
K_2O	6.57	6.35	6.45	7.19	5.96	7.41	6.14	8.03	8.67	8.31
P_2O_5	1.09	0.78	1.26	1.06	0.66	0.56	1.12	1.18	0.53	0.57
LOI	0.54	0.62	1.14	0.90	1.81	0.53	0.73	0.90	1.24	2.81
TOTAL	98.49	99.38	98.11	99.61	96.81	99.56	99.32	97.48	99.01	98.85
K_2O/Na_2O	3.44	2.31	4.36	2.64	4.20	2.38	3.01	4.29	3.22	3.07
Mg#	0.83	0.71	0.80	0.98	0.89	0.89	0.83	0.80	0.79	0.77
(ppm)										
Li	13.2	14.9	28.7	16.2	24.2	37.6	16.4	15.9	25.6	19.4
Be	21.2	10.1	23.7	10.3	11.7	11.7	22.5	28.8	16.1	14.9
Sc	17.5	14.4	19.6	15.0	22.3	12.7	18.6	17.1	8.4	9.4
V	125	116	127	76	125	75	125	114	64	72
Cr	561	103	610	364	401	147	670	266	70	92
Co	58	41	51	43	54	43	55	40	44	43
Ni	372	70	341	209	319	83	395	165	52	64
Cu	52	31	59	33	65	31	42	41	30	27
Zn	79	84	85	70	85	77	79	86	63	64
Ga	20.6	20.4	22.1	21.6	14.6	21.4	20.6	22.6	25.4	24.1
Ge	2.54	1.77	2.87	1.96	1.65	1.93	2.47	2.28	2.35	2.18
Rb	451	487	331	486	298	650	2518	873	435	419
Sr	1144	1260	1343	1020	2169	893	1264	1057	967	1075
Zr	643	525	831	611	283	484	679	809	898	849
Nb	32.7	29.3	43.2	33.6	12.8	30.2	34.6	54.3	60.1	53.8
Cs	52.89	8.88	6.96	10.11	25.88	28.95	348.30	52.64	11.66	16.14
Ba	3387	1853	5513	2984	10170	1737	4044	2893	3038	3354
Hf	18.6	13.8	22.8	19.1	6.7	13.8	19.6	25.1	26.2	24.5
Ta	1.90	1.85	2.44	2.46	0.71	2.13	2.02	3.30	3.42	3.05
Pb	89	41	121	89	284	71	99	133	154	167
Th	215.6	81.2	298.0	123.3	69.6	112.1	239.4	242.0	158.6	139.2
U	32.25	15.97	19.52	20.71	11.38	27.00	33.89	41.13	18.63	16.89
La	126.8	99.5	175.3	100.4	144.0	112.0	146.6	128.4	217.1	204.0
Ce	344	220	455	232	257	243	386	335	433	411
Pr	54.2	30.6	67.2	36.3	33.7	33.5	59.1	52.7	51.6	50.3
Nd	261	124	310	159	133	136	269	239	191	187
Sm	48.6	20.9	59.5	29.0	25.0	24.7	51.6	48.5	25.5	25.6
Eu	7.56	3.64	8.65	4.62	7.46	3.78	7.52	6.80	4.21	4.34
Gd	27.6	14.3	33.2	18.2	20.2	15.7	28.9	28.0	17.8	17.7
Tb	2.69	1.53	3.19	1.96	2.23	1.66	2.79	2.88	1.55	1.56
Dy	9.7	6.5	11.9	8.3	9.6	7.0	10.3	11.0	6.0	6.2
Ho	1.22	1.00	1.44	1.26	1.46	0.99	1.28	1.44	0.77	0.80
Er	3.17	2.57	3.79	3.29	3.55	2.62	3.39	3.67	2.21	2.28
Tm	0.31	0.31	0.37	0.39	0.42	0.30	0.33	0.38	0.23	0.24
Yb	2.10	1.97	2.37	2.54	2.65	1.96	2.15	2.40	1.52	1.57
Lu	0.30	0.29	0.33	0.38	0.39	0.29	0.30	0.35	0.23	0.24
Y	32.2	28.8	39.5	34.1	39.0	27.8	33.6	38.1	20.8	21.6
$^{87}Sr/^{86}Sr$	0.722810	0.716194	0.724697	0.719414	0.715817	0.720068	0.721161	0.736451	0.718431	0.718043
$(^{87}Sr/^{86}Sr)(t)$	0.720572	0.714000	0.723298	0.716384	0.715118	0.716369	0.711454	0.732254	0.715876	0.715778
$^{143}Nd/^{144}Nd$	0.511100	0.511181	0.511085	0.511224	0.511287	0.511179	0.511075	0.511116	0.511192	0.511198
$(^{143}Nd/^{144}Nd)(t)$	0.511090	0.511172	0.511074	0.511213	0.511278	0.511170	0.511066	0.511106	0.511185	0.511190
ε_{Nd} (0)	-14.4	-12.8	-14.7	-12.2	-10.7	-12.8	-14.9	-14.2	-12.6	-12.5
$\varepsilon_{Nd}(t)$	-14.2	-12.6	-14.5	-11.8	-10.6	-12.7	-14.8	-14.0	-12.4	-12.3
T_{DM} (Ga)	1.76	1.49	1.84	1.55	1.51	1.60	1.85	1.92	1.25	1.26
$^{206}Pb/^{204}Pb$	18.7281	19.3452	18.6855	18.9979	18.4494	18.8957	18.7076	18.8374	18.4819	18.4694
$^{207}Pb/^{204}Pb$	15.7666	15.8028	15.7638	15.7851	15.7422	15.7785	15.7621	15.7858	15.7552	15.7485
$^{208}Pb/^{204}Pb$	39.8862	40.1683	39.8417	39.8692	39.4869	39.6104	39.8424	39.8216	39.4794	39.4432
$\delta^{18}O_{SMOW}$ (‰) **	7.8	8.1	8.3	8.5	8.1	9.3	7.6 (8.2)	9.0 (8.1)	7.2 (7.4)	6.3 (8.8)

* Samples with major and trace elements data first published by Nomade et al. (2004).
** The $\delta^{18}O_{SMOW}$ data are from whole rock samples, except for those shown in parentheses that are from phlogopites.

DR03	DR04	Z8030-5	Z8030-18	ZB1 *	ZB3	ZB4 *	ZB6	ZB8	ZB9
Dangreyong	Dangreyong	Dangreyong	Dangreyong	Zabuye	Zabuye	Zabuye	Zabuye	Zabuye	Zabuye
E86°23.5′	E86°23.5′	E86°39.4′	E86°39.4′	84°18.0′	84°18.0′	84°18.0′	84°18.0′	84°18.0′	84°18.0′
N30°56.6′	N30°56.6′	N31°51.0′	N31°51.0′	31°24.1′	31°24.1′	31°24.1′	31°24.1′	31°24.08′	31°24.1′
4751	4751			4602	4654	4662	4672	4678	4680
14.2 ± 0.3	13.5 ± 02	13.47 ± 0.13	13.17 ± 0.11	16.16		16.12			
60.98	59.28	55.96	55.23	56.44	56.12	55.90	55.73	56.86	55.04
0.90	0.88	1.37	1.57	1.24	1.24	1.25	1.23	1.23	1.21
13.92	13.92	13.60	13.64	13.48	13.45	13.52	13.46	13.75	13.17
3.98	3.95	4.47	5.92	6.53	6.59	6.46	6.46	6.48	6.38
1.45	1.40	1.30	2.32	1.32	2.42	2.42	2.55	1.75	1.70
0.06	0.06	0.06	0.07	0.09	0.10	0.09	0.10	0.10	0.09
2.53	2.62	4.12	4.75	4.21	4.98	4.32	4.88	4.90	4.90
3.29	2.92	4.39	4.90	5.93	6.19	5.92	6.59	6.08	7.03
2.59	2.37	2.53	2.08	3.14	3.15	3.12	3.18	3.14	2.97
8.46	8.83	7.47	7.77	6.53	6.24	6.41	6.18	6.32	6.11
0.54	0.56	0.68	0.67	1.16	1.12	1.12	1.10	1.12	1.11
2.27	2.74	2.95	0.80	0.76	0.39	0.73	1.07	0.39	1.51
99.52	98.13	97.60	97.40	99.51	99.57	98.84	99.98	100.37	99.52
3.27	3.73	2.95	3.74	2.08	1.98	2.05	1.94	2.01	2.06
0.76	0.77	0.85	0.78	0.85	0.79	0.76	0.77	0.83	0.84
32.7	25.0	24.8	11.6	14.8	20.6	20.4	24.1	20.8	23.5
16.2	16.5	9.1	15.7	7.2	8.9	7.9	8.7	8.5	9.7
8.6	9.4	12.9	16.2	12.20	14.34	13.61	14.41	13.92	13.62
65	76	95	130	113.2	139.6	123.9	130.4	129.3	127.3
74	82	213	229	126	126	138	130	135	132
54	54	29	37	15	22	20	20	21	21
53	61	124	141	82.9	89.1	92.0	87.3	92.4	89.6
29	29	31	34	68	47	71	57	65	64
62	66	81	89	87	94	90	93	105	101
24.9	25.5	28.4	26.6	17.3	20.2	20.6	19.8	20.4	19.8
2.34	2.37	2.72	2.55	1.61	1.99	1.93	1.94	1.97	1.97
416	459	1574	595	350	359	379	349	356	337
1283	1286	1226	1225	1441	1673	1638	1620	1695	1682
903	868	870	794	298	333	335	324	334	334
58.5	52.8	55.8	35.3	34.1	36.6	38.3	37.8	38.5	35.6
13.25	14.56	24.10	7.39	13.70	13.64	13.43	15.34	9.65	23.15
3299	3966	2760	2751	2507	2698	2823	2656	2858	2719
26.7	24.0	26.0	23.1	8.4	9.3	9.6	9.2	9.3	9.1
3.36	3.13	3.19	2.24	1.78	1.89	2.01	1.99	1.98	1.88
182	220	121	95	77	82	79	87	88	81
152.4	172.2	100.8	173.8	55.6	59.7	63.7	61.2	61.9	59.5
18.21	19.40	7.45	16.66	14.74	14.37	14.81	14.05	14.01	14.88
208.4	220.7	209.8	148.5	62.2	68.9	72.0	67.9	70.1	67.5
416	446	419	354	122	135	139	135	138	136
50.7	49.0	53.7	49.5	19.8	21.7	22.8	21.7	22.1	21.6
188	177	199	209	87	94	98	93	96	93
25.2	23.7	25.5	34.1	16.8	18.1	19.1	18.1	18.7	17.9
4.22	4.25	3.83	5.01	3.27	3.55	3.67	3.51	3.67	3.56
17.6	16.6	18.1	19.8	10.9	12.0	12.4	11.9	12.3	11.9
1.54	1.44	1.57	1.86	1.20	1.32	1.35	1.29	1.34	1.28
5.9	5.7	6.1	7.3	5.3	5.8	5.9	5.7	5.9	5.8
0.77	0.74	0.77	1.00	0.78	0.89	0.88	0.85	0.86	0.85
2.21	2.03	2.23	2.58	2.03	2.25	2.29	2.22	2.25	2.20
0.24	0.23	0.23	0.30	0.25	0.29	0.28	0.28	0.28	0.27
1.54	1.52	1.47	1.94	1.66	1.89	1.88	1.81	1.86	1.82
0.23	0.22	0.22	0.28	0.24	0.27	0.27	0.28	0.26	0.26
20.5	20.9	20.0	27.4	26.0	29.1	28.5	27.9	28.7	27.5
0.718299		0.723137	0.719632	0.711352	0.710890	0.711075	0.711118	0.711039	0.710719
0.716347		0.714977	0.716543	0.709703	0.709434	0.709508	0.709656	0.709616	0.709362
0.511182		0.511134	0.511138	0.511388	0.511410	0.511422	0.511408	0.511440	0.511435
0.511174		0.511126	0.511128	0.511375	0.511397	0.511409	0.511395	0.511428	0.511423
-12.8		-13.7	-13.6	-8.8	-8.3	-8.1	-8.4	-7.7	-7.8
-12.6		-13.5	-13.5	-8.6	-8.2	-7.9	-8.2	-7.6	-7.7
1.26		1.28	1.50	1.41	1.37	1.35	1.43	1.31	1.26
18.4787		18.522		18.827	18.790				
15.754		15.7553		15.778	15.746				
39.4705		39.5556		39.573	39.521				
6.9 (7.8)		9.1		9.0	8.5	9.4 (8.7)	8.7	9.3	9.2

(continued on next page)

Table 6 (*continued*)

Sample	ZB10 *	ZB11	ZB12 *	ZB14	ZB16	ZB18	ZB20	ZB21	ZB22	SL0618
Locality	Zabuye	Zabuye	Zabuye	Zabuye	Zabuye	Zabuye	Zabuye	Zabuye	Zabuye	Sailipu
Longtitude	84°18.0′	84°18.0′	84°18.0′	84°18.0′	84°18.0′	84°18.1′	84°18.1′	84°23.3′	84°23.3′	82°58.5′
Latitude	31°24.1′	31°24.1′	31°24.1′	31°24.1′	31°24.1′	31°24.2′	31°24.2′	31°27.7′	31°27.7′	31°17.8′
Altitude (m)	4683	4694	4705	4721	4753	4810				4864
Age (Ma)	16.1		16.1					27.14 ± 0.05		
(wt.%)										
SiO_2	56.48	55.98	57.13	57.69	57.67	55.52	55.29	55.02	58.31	58.9
TiO_2	1.23	1.24	1.25	1.18	1.18	1.27	1.25	1.35	1.27	1.3
Al_2O_3	13.51	13.55	13.71	13.77	13.83	13.44	13.31	14.40	14.94	13.9
TFe_2O_3	6.58	6.57	6.22	6.05	6.08	6.44	6.44	7.14	6.24	5.7
FeO	1.42	1.62	1.05	1.20	2.22	2.58	2.00	2.78	0.10	5.1
MnO	0.10	0.10	0.09	0.08	0.09	0.10	0.09	0.13	0.11	0.1
MgO	4.46	4.94	4.10	3.93	4.17	4.52	4.43	2.59	2.93	5.5
CaO	6.22	6.24	5.62	5.30	5.38	6.48	6.88	3.65	2.76	4.9
Na_2O	3.08	3.06	3.25	3.41	3.31	3.11	3.04	2.98	3.92	2.5
K_2O	6.32	6.24	6.54	6.60	6.54	6.42	6.31	8.77	7.83	5.6
P_2O_5	1.13	1.12	0.98	0.93	0.95	1.09	1.08	0.65	0.71	0.7
LOI	0.64	0.68	0.77	1.02	0.46	1.12	1.68	1.86	0.70	0.7
TOTAL	99.75	99.70	99.66	99.96	99.66	99.51	99.80	98.54	99.72	99.8
K_2O/Na_2O	2.05	2.04	2.01	1.94	1.98	2.06	2.08	2.94	2.00	2.2
Mg#	0.85	0.84	0.87	0.85	0.77	0.76	0.80	0.62	0.98	0.66
(ppm)										
Li	19.7	21.0	31.2	38.2	30.0	29.0	27.5	68.6	31.1	
Be	8.7	9.2	13.3	12.5	12.0	11.6	11.6	30.8	30.6	10.7
Sc	13.30	13.70	12.59	11.95	11.87	13.14	13.72	10.5	10.2	14.6
V	125.1	127.3	112.5	106.5	114.6	128.1	128.6	121	106	114
Cr	145	138	116	106	106	116	117	52	53	235
Co	21	21	17	16	17	18	18	33	56	23
Ni	96.3	92.2	72.4	73.6	71.1	66.8	67.4	40	44	133
Cu	67	58	72	78	55	36	46	39	26	23
Zn	92	102	105	95	96	98	99	121	91	79
Ga	19.6	20.4	20.9	21.7	21.0	20.5	19.9	25.1	24.7	21.7
Ge	1.91	2.00	1.94	1.91	2.00	1.96	1.89	1.94	1.70	
Rb	357	354	425	450	420	442	443	788	669	494
Sr	1626	1700	1495	1489	1504	1544	1497	1315	872	888
Zr	334	341	424	442	440	388	378	1433	1001	527
Nb	36.2	37.0	50.0	52.2	50.6	48.2	47.9	122	77.4	26.7
Cs	12.26	23.56	29.05	17.67	18.08	18.97	26.87	100.62	65.24	14.57
Ba	2775	2859	2919	2871	2899	2743	2661	3087	2231	2542
Hf	9.2	9.4	11.9	12.0	12.1	10.8	10.6	38.8	27.6	14.0
Ta	1.88	1.94	2.77	2.81	2.80	2.58	2.56	7.79	3.85	1.47
Pb	78	87	119	111	90	83	82	169	126	57
Th	59.0	61.0	94.4	96.0	97.5	82.9	82.9	322.5	264.6	179
U	15.66	14.39	20.88	23.57	23.88	24.11	22.26	76.18	55.21	20.76
La	67.6	68.1	69.4	69.5	69.1	68.4	67.4	123.9	106.8	124.6
Ce	136	139	138	138	139	138	140	265	225	311
Pr	21.7	21.9	21.7	21.2	21.2	21.7	21.6	35.8	30.5	42.7
Nd	93	95	91	89	89	93	92	141	120	178
Sm	18.0	18.3	17.9	17.0	17.2	17.9	17.6	26.3	21.9	33.0
Eu	3.58	3.60	3.54	3.37	3.41	3.54	3.52	5.07	4.16	5.31
Gd	11.9	12.0	12.0	11.4	11.5	12.0	11.8	18.2	15.2	16.6
Tb	1.31	1.33	1.33	1.28	1.29	1.35	1.30	2.06	1.68	1.57
Dy	5.8	5.9	6.1	5.7	5.9	6.0	5.9	8.9	7.2	5.9
Ho	0.86	0.88	0.90	0.87	0.86	0.90	0.88	1.34	1.11	0.90
Er	2.23	2.27	2.29	2.23	2.23	2.33	2.27	3.41	2.89	2.26
Tm	0.28	0.29	0.29	0.29	0.29	0.29	0.29	0.44	0.37	0.27
Yb	1.86	1.87	1.92	1.89	1.86	1.90	1.92	2.94	2.47	1.69
Lu	0.26	0.27	0.27	0.26	0.27	0.28	0.28	0.45	0.38	0.23
Y	27.5	28.2	29.2	28.2	28.4	29.6	28.8	34.8	29.7	25.2
$^{87}Sr/^{86}Sr$	0.710866	0.712071	0.712408	0.712063	0.712089	0.711987	0.711992	0.714894	0.714686	0.719001
$(^{87}Sr/^{86}Sr)(t)$	0.709376	0.710660	0.710480	0.710016	0.710197	0.710047	0.709984	0.707995	0.705858	0.714757
$^{143}Nd/^{144}Nd$	0.511447	0.511443	0.511433	0.511403	0.511442	0.511428	0.511434	0.511333	0.511345	0.511876
$(^{143}Nd/^{144}Nd)(t)$	0.511434	0.511430	0.511420	0.511390	0.511429	0.511415	0.511420	0.511312	0.511325	0.511862
ε_{Nd} (0)	-7.6	-7.7	-7.9	-8.5	-7.7	-8.0	-7.9	-9.8	-9.6	-14.9
$\varepsilon_{Nd}(t)$	-7.4	-7.5	-7.7	-8.3	-7.5	-7.8	-7.7	-9.6	-9.3	-14.7
T_{DM} (Ga)	1.34	1.34	1.38	1.39	1.36	1.33	1.48	1.43	1.38	2.00
$^{206}Pb/^{204}Pb$	18.799			18.795		18.857	18.812	18.9587	18.9158	18.5982
$^{207}Pb/^{204}Pb$	15.744			15.748		15.802	15.734	15.769	15.7718	15.7219
$^{208}Pb/^{204}Pb$	39.463			39.500		39.689	39.540	39.9286	39.8985	39.6373
$\delta^{18}O_{SMOW}$ (‰) **	9.1	9.3	9.5	9.2	8.9	9.2	10.3	8.3	6.7	9.3

SL0619	SL0620	SL0621	SL0622	SL0623	SL0624	SL0625	SL0628	SL0630	SL0631
Sailipu	Sailipu	Sailipu	Sailipu	Sailipu	Sailipu	Sailipu	Sailipu	Sailipu	Sailipu
82°58.5′	82°58.5′	82°58.5′	82°58.5′	82°58.5′	82°58.5′	82°58.5′	82°58.5′	82°58.5′	82°58.5′
31°17.8′	31°17.8′	31°17.8′	31°17.8′	31°17.8′	31°17.8′	31°17.8′	31°17.8′	31°17.8′	31°17.8′
4864	4864	4864	4864	4864	4864	4864	4864	4864	4864
							17.7 ± 0.3		
58.84	59.0	54.6	57.9	56.4	56.8	56.7	60.61	54.07	55.7
1.35	1.3	1.4	1.4	1.3	1.4	1.4	1.22	1.59	1.4
14.00	13.7	13.0	14.4	12.1	12.1	13.5	14.53	12.50	13.6
5.63	5.5	6.8	5.8	6.4	6.5	6.6	5.76	6.72	6.8
5.1	5.0	6.1	5.2	5.8	5.9	6.0	5.2	6.0	6.1
0.11	0.1	0.1	0.1	0.1	0.1	0.1	0.06	0.10	0.1
5.33	5.4	9.0	5.3	8.9	9.3	6.2	4.18	9.51	7.5
4.80	4.8	5.5	4.9	5.2	5.1	5.0	4.71	5.45	5.7
2.45	2.2	1.7	2.5	1.6	1.7	2.2	2.75	1.69	2.5
5.67	5.9	5.9	5.7	5.9	5.9	5.7	4.66	6.60	5.3
0.71	0.7	0.9	0.8	0.8	0.8	0.8	0.57	0.94	0.8
0.94	1.3	0.7	0.8	0.9	0.1	1.5	1.26	0.47	0.4
99.83	99.9	99.7	99.5	99.5	99.8	99.8	100.31	99.64	99.8
2.31	2.7	3.4	2.3	3.7	3.4	2.6	1.69	3.91	2.1
0.65	0.66	0.72	0.64	0.73	0.74	0.65	0.59	0.74	0.66
11.2	11.4	11.3	11.3	10.7	10.9	10.2	6.3	11.3	10.4
14.48	14.4	18.7	14.8	17.7	17.3	17.8	14.08	18.25	17.3
112.76	112	138	110	128	130	130	107.55	144.69	144
227	232	470	236	459	426	364	196	496	368
23	21	33	23	33	31	28	19	33	30
142.03	119	283	138	309	252	124	105.89	144.46	209
25	24	29	33	42	34	34	33	20	28
83	81	86	83	78	77	95	86	85	86
22.14	21.5	21.0	22.2	19.6	20.1	21.3	20.99	22.09	21.4
497	533	389	469	499	583	507	391	601	434
893	870	942	896	814	873	761	787	939	1003
528	519	568	534	540	562	517	381	621	491
26.96	25.9	33.9	26.6	31.4	30.7	30.7	22.13	34.48	29.6
16.65	20.61	10.69	6.04	17.72	24.75	14.45	13.15	8.12	9.60
2583.01	2504	2474	2549	2084	2310	2137	1692.19	2480.37	2269
14.1	13.5	15.7	13.9	14.7	15.3	13.9	9.8	16.9	13.0
1.47	1.40	1.89	1.46	1.75	1.73	1.64	1.20	1.88	1.60
62	58	56	68	49	50	44	36	44	49
178.91	171	189	178	174	188	147	105.23	217.61	170
19.94	20.74	21.82	20.00	21.68	23.65	19.22	13.25	25.01	19.92
126.2	119.9	104.1	125.8	97.4	102.8	98.6	83.7	118.5	102.4
307	288	271	307	258	266	232	185	310	257
43.0	39.7	37.8	42.7	36.1	37.8	32.8	25.2	46.3	36.0
177	171	169	180	162	168	142	107	206	156
32.6	31.0	31.9	33.0	29.9	32.1	26.5	19.1	40.0	29.7
5.29	5.07	5.00	5.39	4.52	4.96	4.15	3.24	6.11	4.80
16.4	15.9	16.0	16.9	14.6	15.6	13.9	10.0	19.5	15.1
1.57	1.51	1.58	1.59	1.45	1.53	1.39	1.04	1.83	1.44
5.8	5.7	6.4	6.1	5.9	6.2	5.9	4.5	7.3	5.9
0.88	0.87	1.07	0.96	0.96	0.99	0.97	0.78	1.12	0.93
2.22	2.21	2.70	2.31	2.48	2.59	2.52	1.98	2.74	2.33
0.27	0.27	0.34	0.29	0.32	0.33	0.32	0.26	0.35	0.29
1.73	1.63	2.19	1.78	1.88	2.03	1.94	1.57	2.13	1.71
0.24	0.23	0.29	0.25	0.27	0.28	0.28	0.23	0.29	0.23
24.8	25.0	29.5	27.2	26.2	27.2	28.2	20.4	30.4	25.1
	0.718777	0.719090	0.718705	0.719828	0.718913	0.717691			0.716394
	0.714103	0.715936	0.714715	0.715151	0.713816	0.712609			0.713095
	0.511890	0.511876	0.511887	0.511867	0.511872	0.511911			0.511899
	0.511877	0.511862	0.511873	0.511853	0.511858	0.511897			0.511885
	-14.6	-14.9	-14.6	-15.0	-14.9	-14.2			-14.4
	-14.4	-14.7	-14.5	-14.9	-14.8	-14.0			-14.2
	1.93	2.03	1.95	2.00	2.08	1.95			2.02
	18.5970	18.6399	18.5846	18.6619	18.6250	18.7056			18.6397
	15.7221	15.7231	15.7165	15.7343	15.7307	15.7591			15.7288
	39.6306	39.6075	39.5954	39.6299	39.6424	39.6898			39.6491
	9.2	8.9	9.3	9.0	9.1	9.4			7.7

ultrapotassic rocks. Thus, we do not separate these five samples from the others (Fig. 4a, b). All of the samples plot between Groups I (lamproite) and III (orogenic, lamprophyre-like) in the ultrapotassic discrimination diagrams (Fig. 5a, b; Foley et al., 1987). The transitional nature of these rocks was also noted by Miller et al. (1999) and Gao et al. (2007a).

Most of the analyzed rocks are trachyandesite and trachyte, accompanied by minor basaltic trachyandesite, tephriphonolite and tephrite (Fig. 4a). In the plot of K_2O vs. Na_2O (Fig. 4b), most of the samples lie within the ultrapotassic field. Those from Zabuye salt lake lie on or close to the boundary and one sample from Sailipu, lies in the shoshonite field.

In plots of various elements against MgO (Fig. 6), most oxides show linear trends, particularly for samples from a particular locality. Silica, Al_2O_3, Na_2O, and K_2O, correlate negatively with MgO, whereas $Fe_2O_{3(t)}$, TiO_2 and CaO correlate positively. The LOI (loss on ignition) is relatively low and reflects the abundance of phlogopite in the rock rather than alteration. It generally decreases with increasing MgO (Fig. 6f). The high MgO samples in Gongmutang contain abundant olivine and clinopyroxene, with rare phlogopite. No clear correlations exist between LILE (Ba, Rb, and Sr) and MgO content (Fig. 6j to l). In general, the K_2O/Na_2O ratios increase with increasing MgO (Fig. 6i).

All of the analyzed samples are strongly enriched in light REE (La: 200 to 711 times chondrite, $[La/Yb]_N = 24–98$, where the subscript 'N' denotes normalization to chondrite values) and most show well-developed negative Eu anomalies (Fig. 7a). The rocks have generally high Rb (298–2518 ppm), Cs (6–348 ppm), Sr (761–1700 ppm), Ba (1692–10,170 ppm), and Th (56–323 ppm) (Table 7). Their primitive mantle-normalized spider diagrams show positive anomalies for Rb, Th, Pb, Nd and Sm, and marked negative anomalies for Ba, Sr, P and HFSE, particularly Ti, Nb, and Ta (Fig. 7b). The rocks have very radiogenic Sr ($^{87}Sr/^{86}Sr_{(i)} = 0.710719$ to 0.736451), unradiogenic Nd ($\varepsilon_{Nd(0)} = -7.6$ to -15), and fairly radiogenic Pb isotopic signatures ($^{206}Pb/^{204}Pb = 18.449–19.345$, $^{207}Pb/^{204}Pb = 15.717–15.803$, $^{208}Pb/^{204}Pb = 39.443–40.168$), indicating that they originated from an enriched upper mantle source with a composition close to that of EM II (Figs. 8 and 9). This implies that the source region was contaminated by old ($T_{DM} = 1.3–2.1$ Ga) continental materials, which were recycled into the ultrapotassic rocks (e.g., Turner et al., 1993, 1996; Miller et al., 1999; Ding et al., 2003; Williams et al., 2004; Ding et al., 2006; Gao et al., 2007a). The same situation was found in Italy (e.g., Conticelli and Peccerillo, 1992; Conticelli, 1998; Battistini et al., 2001; Conticelli et al., 2002) and the United States (Davis et al., 1996). The low SiO_2 contents (~45–62 wt.%), high Mg-numbers (56–76) and high Ni and Cr contents (up to 395 ppm and 670 ppm, respectively) in the rocks clearly indicate derivation from the mantle; however, both the elemental and isotopic character of the Tibetan ultrapotassic rocks reflect extensive crustal contamination of the mantle source region. Whole-rock oxygen isotope values ($\delta^{18}O_{SMOW}$) range from 6.3‰ to 10.3‰, whereas those of phlogopite range from 7.4‰ to 8.8‰, indicating a mantle affinity (~7.5‰, Blattner et al., 1989, 2002) (Fig. 10). Because the Tibetan rocks are all quite young (<24 Ma), time-corrected Sr ($^{87}Sr/^{86}Sr_{(t)} = 0.709362–0.732254$) and Nd ($\varepsilon_{Nd}(t) = -14.9$ to -7.4) values are the same as their present-day values, so uncorrected Sr–Nd–Pb data are used in the following discussion.

6. Discussion

6.1. Enrichment of the ultrapotassic source region: Sr–Nd–Pb–O isotopic constraints

The ultrapotassic lavas from Gongmutang have basaltic SiO_2 contents (~45–53 wt.%). Most of the samples from Gongmutang, Sailipu basin, and Xuru lake have high Mg-numbers (65–76), high Ni (150–395 ppm) and high Cr (200–670 ppm) (Fig. 11), suggesting that the ultrapotassic rocks was derived from primitive magmas generated from the upper mantle. This interpretation is supported by the presence of mantle xenoliths entrained by the lavas from Sailipu basin (Zhao et al., 2008a,b) and mantle xenocrysts found in the western Lhasa terrane (Miller et al., 1999). Despite the mantle origin of these rocks, they have extremely high contents of LILE (e.g., LREE, Ba, Rb, Sr, Ce, La, U, Th, Pb; Table 7) that exceed upper and middle continental crustal values (Rudnick and Gao, 2003), indicating that they could not have been produced solely by continental crustal assimilation. Likewise, these lavas could not have been generated from the depleted convecting asthenosphere. Based on their elemental and Sr–Nd–Pb–O isotopic signatures they must have formed from a highly enriched upper mantle source (Miller et al., 1999; Williams et al., 2001; Ding et al., 2003; Williams et al., 2004; Gao et al., 2007a). Most workers have concluded that the dual mantle- and crustal-affinities of the ultrapotassic rocks in Tibet can be explained by low degrees of partial melting of a metasomatically enriched upper mantle (Turner et al., 1996; Miller et al., 1999; Williams et al., 2001; Ding et al., 2003; Williams et al., 2004; Guo et al., 2006; Gao et al., 2007a). However, the nature of the enriching agent, the source of the mantle metasomatism, where and when the metasomatism occurred, and the degree of partial melting are still unclear.

The nature of the enriched upper mantle source region beneath northern Tibet (including North Qiangtang, Songpan–Ganzi and North Kunlun terranes) has been studied extensively beginning with the Sino-British and Sino-French collaborative expeditions in the 1980's (e.g. Coulon et al., 1986; Arnund et al., 1992; Turner et al., 1993, 1996; Deng, 1998, Ding et al., 1999, 2003). Turner et al. (1996) suggested that the most probable metasomatic agents were melts and fluids derived

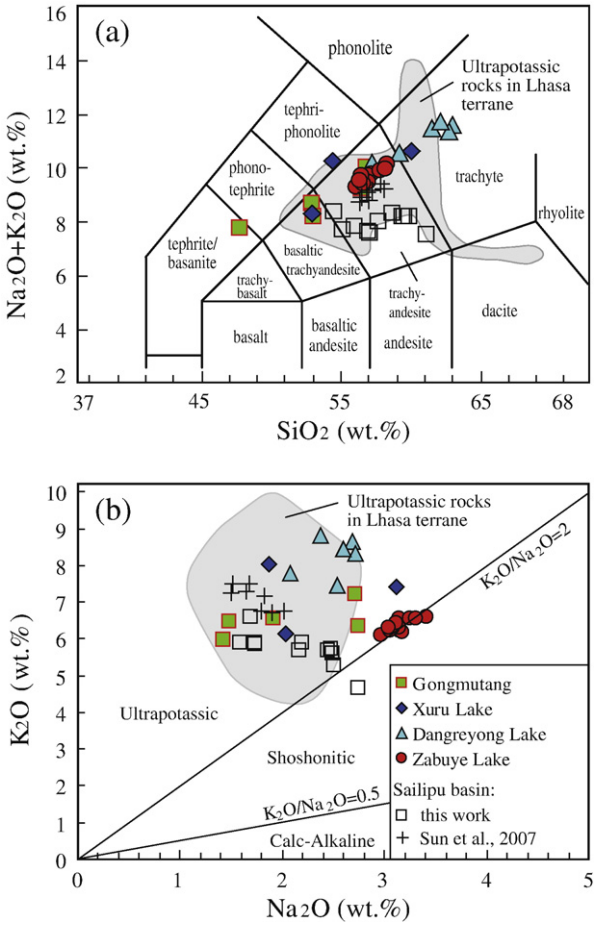

Fig. 4. The ultrapotassic rocks of Tibet plotted on (a) Total alkalis vs. silica, and (b) Potassium vs. sodium, along with published data on ultrapotassic rocks in the Lhasa terrane from Sun et al. (2007), Williams et al. (2004), Ding et al. (2003, 2006), Gao et al. (2007a). Classification scheme is according to Le Maitre (1989).

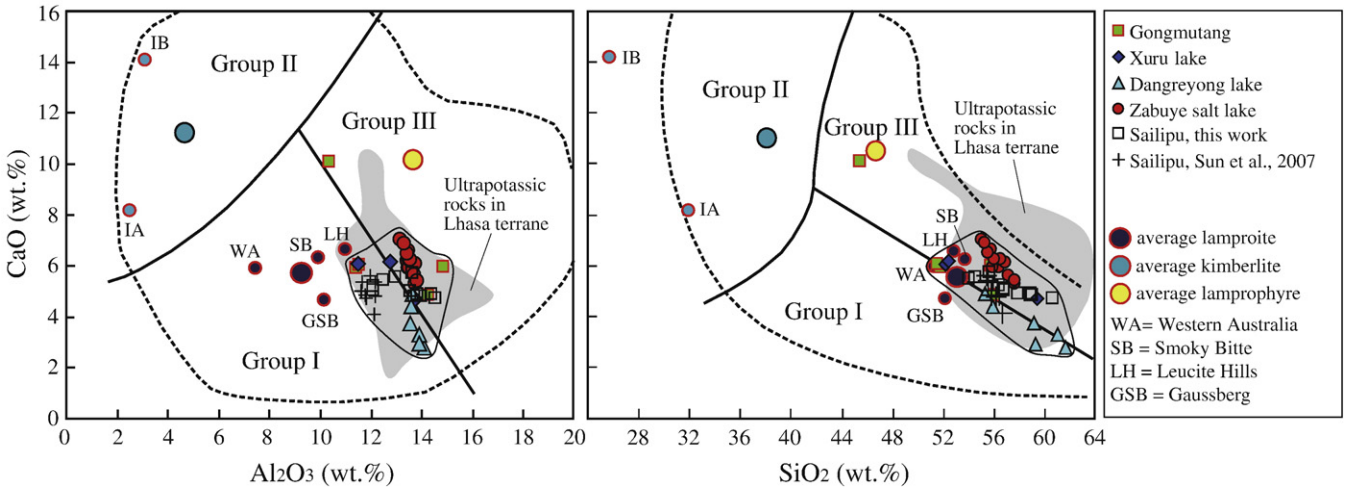

Fig. 5. Discrimination of ultrapotassic magmatic rocks into Groups I, II, and III based on the wt.% CaO vs. Al_2O_3 and SiO_2 (after Foley et al., 1987; Wilson 2001). IA and IB refer to the kimberlites that are totally within cratons and mostly off cratons, respectively. Shaded field shows published data on ultrapotassic rocks in the Lhasa terrane. Data sources as in Fig. 4.

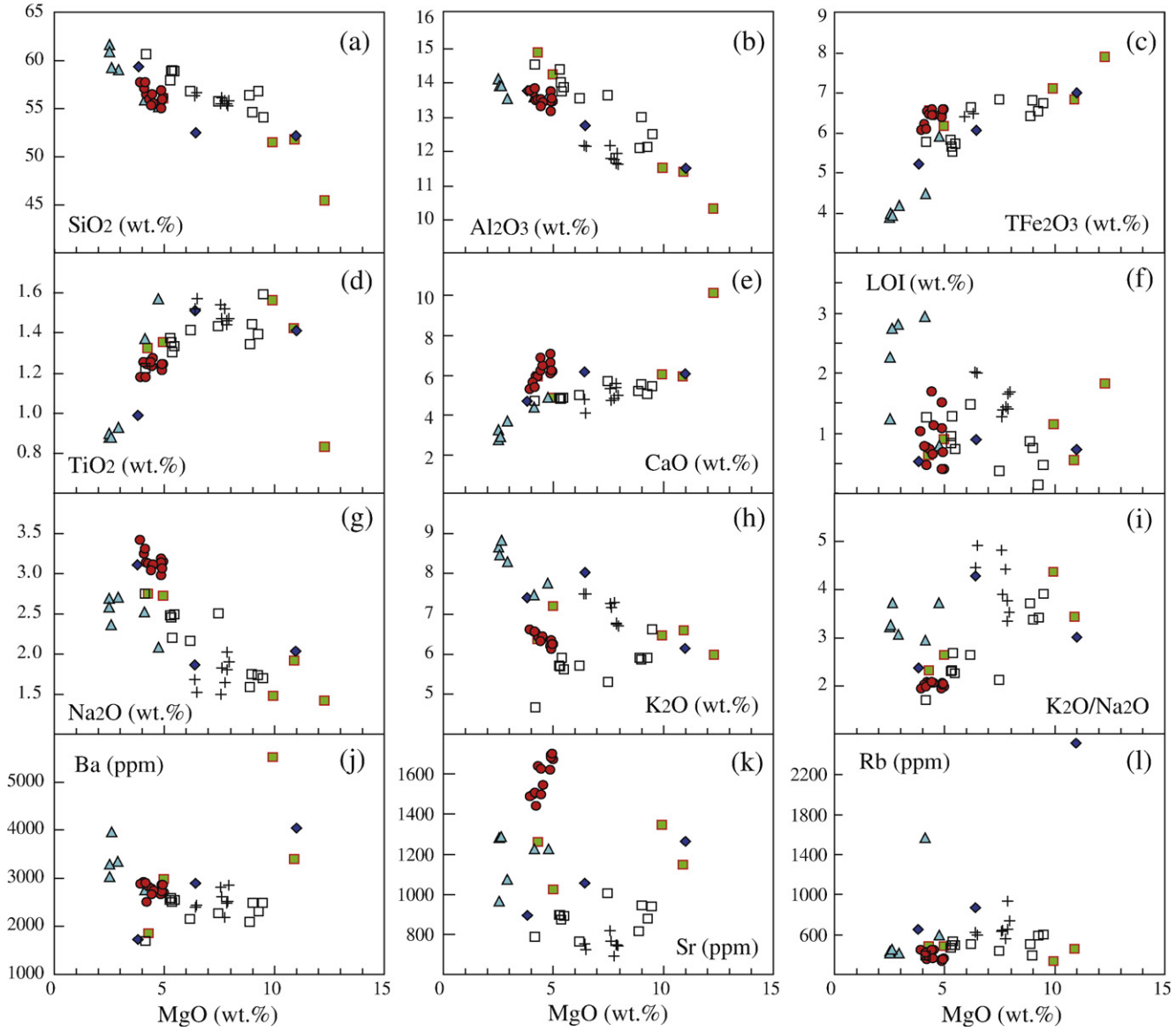

Fig. 6. Harker diagrams showing the variation of selected major oxides (wt.%), trace elements (ppm), major oxide ratios, and LOI (wt.%) against MgO (wt.%) in the ultrapotassic samples. Symbols are as in Fig. 5.

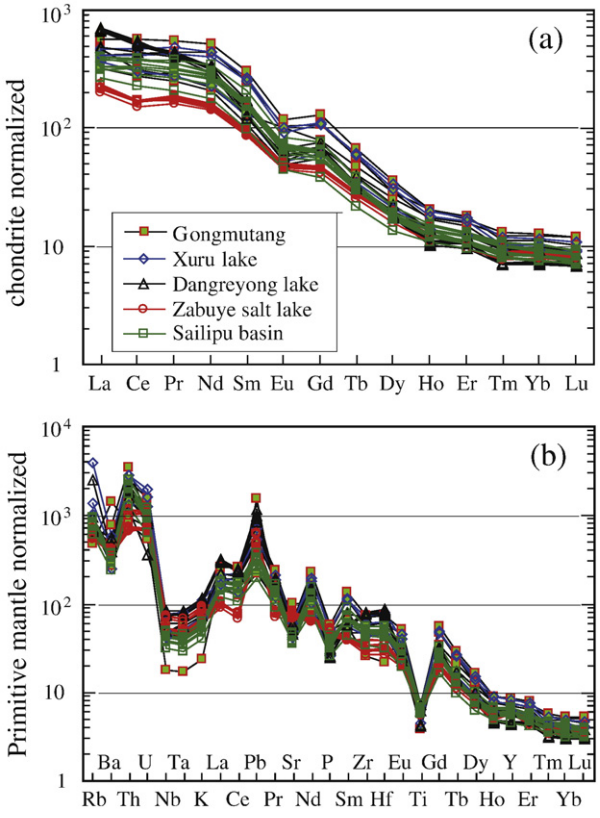

Fig. 7. (a) Chondrite-normalized REE patterns and (b) primitive mantle-normalized trace element patterns for the ultrapotassic samples. Normalizing values in (a) and (b) are from Boynton (1984) and Sun and McDonough (1989), respectively.

from subducted sediments. They also noted a difference between the lavas of the northern and southern plateau based on limited sampling. A recent Sr–Nd–Pb isotopic study by Guo et al. (2006) confirmed that Global Subducting Sediment (GLOSS; Plank and Langmuir, 1998) is the most likely cause of the upper mantle metasomatism. They also note that such metasomatism may have occurred in several stages, an interpretation that is supported by the geochemical and isotopic data of lavas in northern Tibet.

The mantle metasomatism beneath southern Tibet (Lhasa terrane), revealed by the postcollisional ultrapotassic magmatism, may have involved a different type of sediment. For example, Miller et al. (1999) suggested that pelagic sediment is the most suitable candidate for mantle enrichment in the western Lhasa terrane. Based on Pb isotope studies, Gao et al. (2007a) suggested that the mantle enrichment beneath the western Lhasa terrane was related to subduction of Indus river sediments and Indian Ocean turbidites. However, many of the sediments they analyzed have Pb isotopic ratios that are too low to represent the enriched end-member of the ultrapotassic source region. In addition, the extremely high Sr and low Nd isotopes in the lavas are significantly different from the Sr and Nd isotopic character of the Indus River sediments and turbidites. Thus, these sediments are not a good source for the extreme enrichment of the ultrapotassic mantle source. Despite the many studies that support a sediment contamination model, Williams et al. (2004) argue that there are no clear mixing trends between GLOSS and the Tibetan samples, nor can any end-members be identified with the appropriate Sr–Nd–Pb compositions.

In seeking a source for the mantle contamination, most workers have focused on subducted sediments associated with Neo-Tethyan ocean lithosphere. However, Mahéo et al. (2002) suggested that the enrichment was related to subduction of Indian plate continental materials, as India was underthrust beneath Tibet. Using Sr–Nd

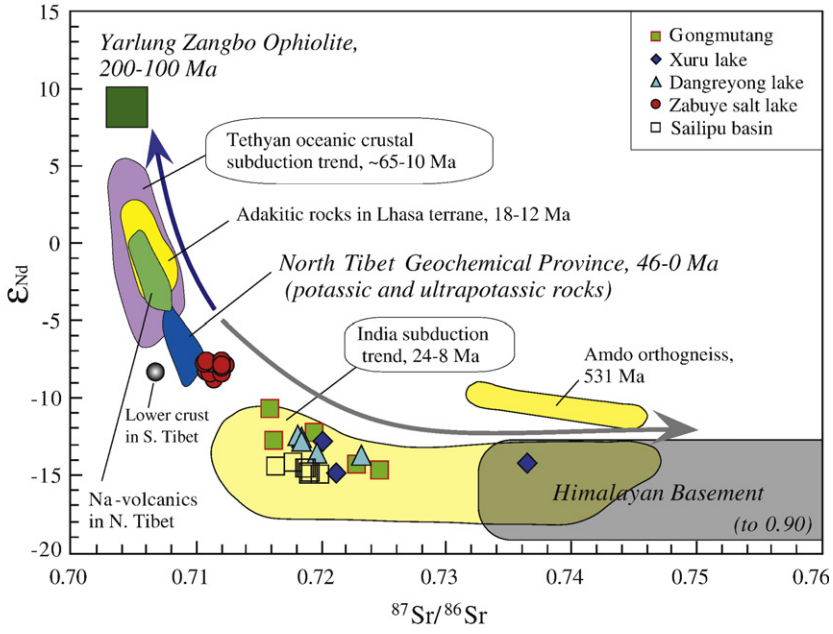

Fig. 8. Plot of ε_{Nd} vs. $^{87}Sr/^{86}Sr$ showing the Sr–Nd features of the ultrapotassic from this work, and other related rocks on the Tibet Plateau. See text for discussion of the three major geochemical end-members and the significant mixing curve between them. The ultrapotassic rocks in the Lhasa terrane lie along a mixing line between North Tibet and the Himalayan basement, indicating that subducted India continental materials were involved in the ultrapotassic magma source region. Data sources: Yarlung Zangbo ophiolite after Miller et al. (2003), Mahoney et al. (2005), Xu and Castillo (2004), Zhang et al. (2005), Niu et al. (2006), Na-volcanic rocks in North Tibet after Deng (1998), Ding et al. (1999), Yang et al. (2002). The shoshonitic and ultrapotassic rocks from North Tibet Geochemical Province are after Yi et al. (2004), Ding et al. (2003), Wang et al. (2005, 2008a,b), Turner et al. (1993, 1996), Deng (1998), Xie (1992), Liu (1989), Cooper et al. (2002), Guo et al. (2006); The Himalayan basement data are after Ahmad et al. (2000), Allègre and Ben Othman (1980), Deniel et al. (1987), Vidal et al. (1982, 1984), Harrison et al. (1999), Inger and Harris (1993), Parrish and Hodges (1996), Robinson et al. (2001), Whittington et al. (1999), Zhang et al. (2004). Published data on the ultrapotassic rocks in Lhasa terrane are as in Fig. 4. Adakitic rocks are after Chung et al. (2003), Hou et al. (2004), Gao et al. (2007b), Guo et al. (2007). Amdo orthogneiss from Harris et al. (1988). Lower crust of South Tibet from Miller et al. (1999). The Tethyan subduction-related rocks (Linzizong volcanic series, Quxu batholith and young ultrapotassic rocks, are from Mo et al. (2007, 2008), Zhao et al. (2001), Turner et al. (1996), Coulon et al. (1986), Miller et al. (1999), Harris et al. (1988), Jiang et al. (1999).

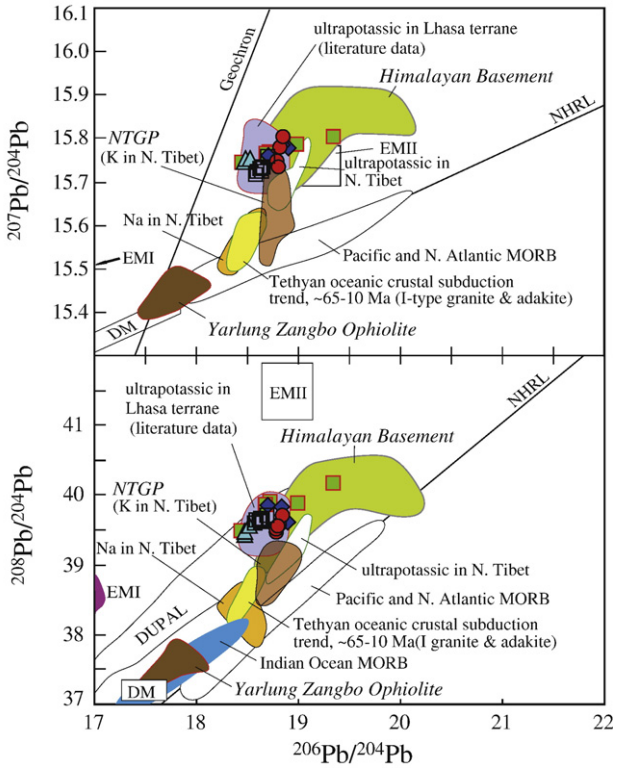

Fig. 9. Plots of $^{207}Pb/^{204}Pb$ and $^{208}Pb/^{204}Pb$, vs. $^{206}Pb/^{204}Pb$ showing the Pb isotopic compositions of ultrapotassic rocks from this work and other related rocks on the Tibetan Plateau. Data sources are as in Fig. 8.

isotopic data for the High Himalayan Crystallines, they suggested that the southern Tibet upper mantle had been metasomatised by melts derived from subducted Indian continental material during slab breakoff. But, as pointed out by Williams et al. (2004), this hypothesis is difficult to confirm by simple Sr–Nd modeling. Williams et al. (2004) further suggested that either subduction of sediments or Indian plate continental materials could have been responsible for the mantle metasomatism and that more data are needed to distinguish these two models.

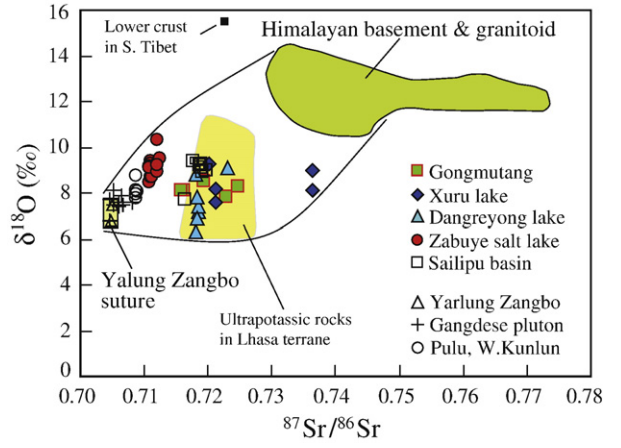

Fig. 10. Plots of oxygen ($\delta^{18}O_{SMOW}$, in ‰) vs. $^{87}Sr/^{86}Sr$ of the ultrapotassic rocks from this work and other related rocks in Tibet. Values for the gabbro from the Yarlung Zangbo suture and the Gangdese pluton are from Debon et al. (1986). Basaltic samples of Pulu from West Kunlun are after Xie (1992). Ultrapotassic rocks and lower crust gabbro from western Lhasa after Miller et al. (1999). The Himalayan basement and granitoids after Debon et al. (1986), Blattner et al. (1983), Deniel et al. (1987), Vidal et al. (1982), France-Lanord et al. (1988).

Our studies (Zhao et al., 2003a,b) and Ding et al. (2003), support involvement of the Himalayan basement in metasomatism of the Tibetan mantle. Ding et al. (2003) suggested that the High Himalayan Crystallines were responsible for Sr–Nd enrichment of the mantle, but they did not consider the Pb and O isotopes or the trace elements involved. Zhao et al. (2003a,b) point out that the systematic Sr–Nd–Pb–O isotopic data of the ultrapotassic lavas can best be explained by underthrusting of the Indian continent beneath southern Tibet. Our current study supports this model, and suggests that subduction of Himalayan continental materials can explain both the geochemical and Sr–Nd–Pb–O isotopic compositions of the lavas. In Figs. 8, 9 and 10, the studied samples lie along a clear trend toward the Himalayan basement. The Himalayan basement rocks have much higher Sr, Pb, and O isotope ratios, and much lower Nd isotopic ratios, than the Tethyan sediments proposed by Gao et al. (2007a) as a source of mantle enrichment.

It is also possible that mature continental crust within the Lhasa terrane might have been responsible for the mantle enrichment. However, based on limited data to date for the Amdo orthogneiss (Harris et al., 1988; Guynn et al., 2006) and the gabbroic lower crust exposed in the western Lhasa terrane (Miller et al., 1999), we infer that there are no basement rocks in the region that have Sr–Nd compositions that can account for the degree of mantle enrichment (Fig. 8).

6.2. Enrichment and partial melting processes — trace element evidence

The ultrapotassic lavas in the Lhasa terrane have trace element compositions similar to those of normal continental arc magmas, with

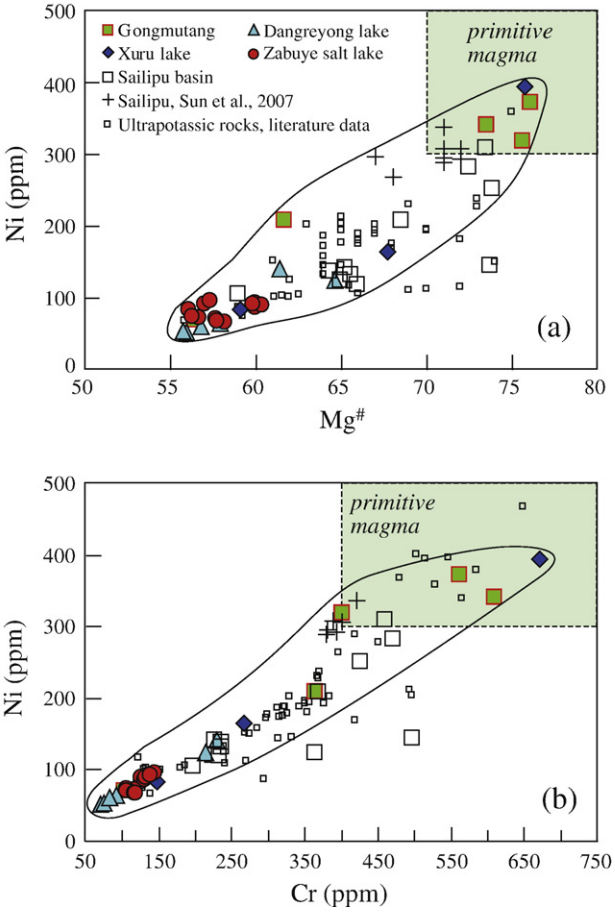

Fig. 11. Plots of Ni (ppm) vs. Mg-number (a) and Cr (ppm) (b) in the ultrapotassic lavas in this work. The sources for published UPV data are as in Fig. 4. Primitive magma field is from Wilson (2001).

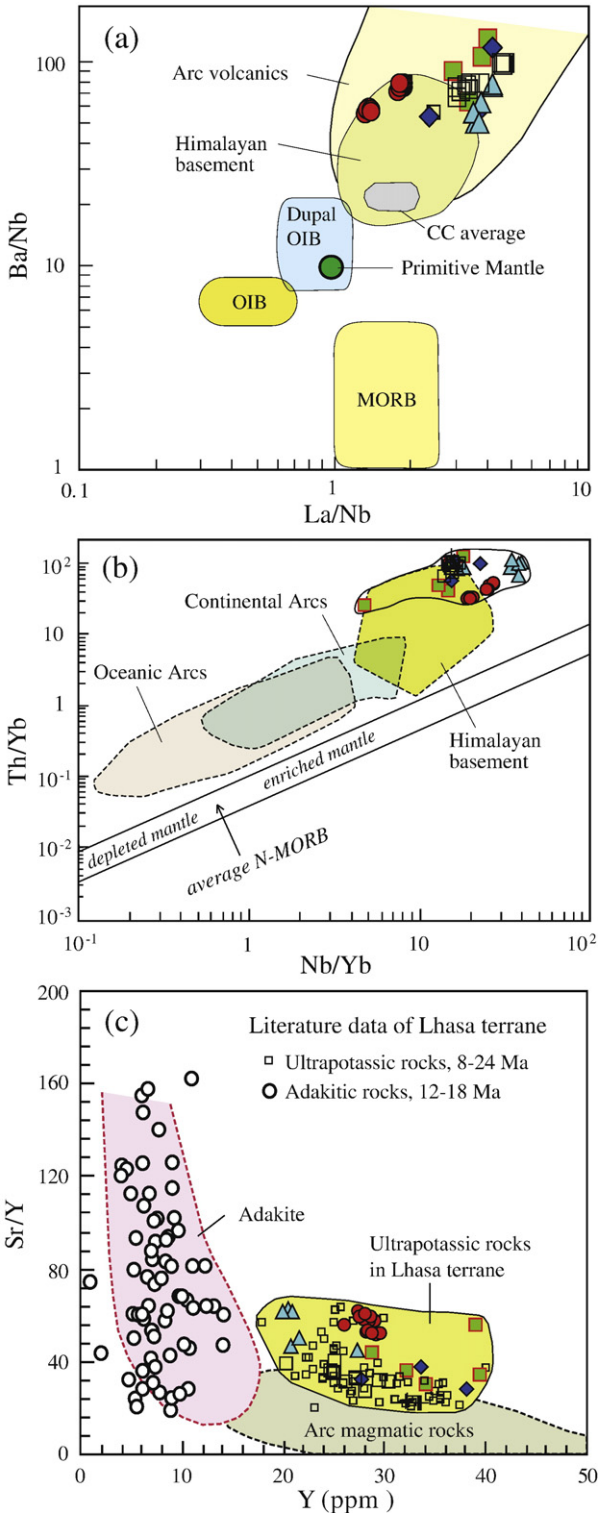

Fig. 12. Trace element plots of (a) Ba/Nb vs. La/Nb, (b) Th/Yb vs. Nb/Yb, and (c) Sr/Y vs. Y in the ultrapotassic lavas. The compositions of different end members in (a) and (b) are after Wilson (2001). The range of adakite and arc magmatic rocks is after Defant et al. (2002). Adakitic rocks and published ultrapotassic data from the Lhasa terrane are as in Figs. 8 and 4, respectively.

enrichment in LILE, LREE and depletion of HFSE (Fig. 7). They are also similar to the shoshonitic and ultrapotassic rocks in northern Tibet (Coulon et al., 1986; Arnund et al., 1992; Turner et al., 1993, 1996; Deng, 1998; Ding et al., 1999, 2003; Guo et al., 2006) and on the eastern margin of the Tibetan plateau (Xu et al., 2001), which have typical "subduction signatures" (Williams et al., 2004). In various trace element plots (Fig. 12), the Tibetan ultrapotassic lavas overlap with the fields of continental arc volcanic rocks in Th, Ba, Nb, and Yb (Fig. 12a, b) and Sr and Y (Fig. 12c) compositions. The Himalayan basement, which is also shown in the plots, is compositionally similar to average continental crust, indicating that it is the best candidate for enrichment of the source region. Despite the similarities between the ultrapotassic and arc magmatism, the former were not generated in a typical continental arc setting, rather they were erupted in the post-collisional, intra-plate setting of the Lhasa terrane following the India–Asia collision at ~65 Ma.

It is not surprising that magmas influenced by subduction of continental materials are compositionally similar to normal subduction-related, arc-type magmas (Elburg and Kamenetsky, 2008), because the enrichment may reflect involvement of continental crust in both cases. If we compare arc-related magmatism and continental crustal material, we see that the nature of the subducted material is more important than the tectonic setting, in which the rocks are formed.

An interesting point is also shown in the Sr/Y vs. Y plot (Fig. 12c), which is widely used to separate adakitic and arc-related rocks (Defant et al., 2002). The ultrapotassic lavas in the western Lhasa terrane are distinctly different from adakitic rocks (12–18 Ma; Chung et al., 2003; Hou et al., 2004; Gao et al., 2007b; Guo et al., 2007), but partially overlap the field of arc-related rocks attributed to Tethyan oceanic subduction (such as the ~65–48 Ma Lizizong volcanic rocks and the ~55–45 Ma southern Gangdese batholith; Dong et al., 2005; Mo et al., 2005; Dong et al., 2006; Mo et al., 2007, 2008; Wen et al., 2008). Although the ultrapotassic magmas were erupted synchronously with the adakitic intrusives, their moderate Sr/Y ratios and relatively high Y indicate that they were derived from a different mantle source. The low Y contents of the adakitic rocks are believed to be due to the presence of residual garnet in the source region (Defant et al., 2002). In contrast, the arc magmas with high Y formed in a garnet-absent environment. However, based on their REE contents, the Tibetan ultrapotassic lavas are believed by some researchers to have originated from a phlogopite-garnet enriched mantle (Fig. 13) (Miller et al., 1999; Xu et al., 2001; Ding et al., 2003; Gao et al., 2007a, b). Trace element modeling by Williams et al. (2004) suggests that garnet should not be a residual mineral in the source region. Nevertheless, different types of post-collisional magmatism overlap spatially and temporally in the Lhasa terrane, as they do in the Roman Magmatic Province of Italy (Conticelli et al., 2002, 2009), indicating the complexity of deep lithospheric processes and materials. Clearly, more detailed work is needed on these rocks and on the collisional orogenic belts between India–Asia plates, before we can fully understand the genesis of the ultrapotassic rocks.

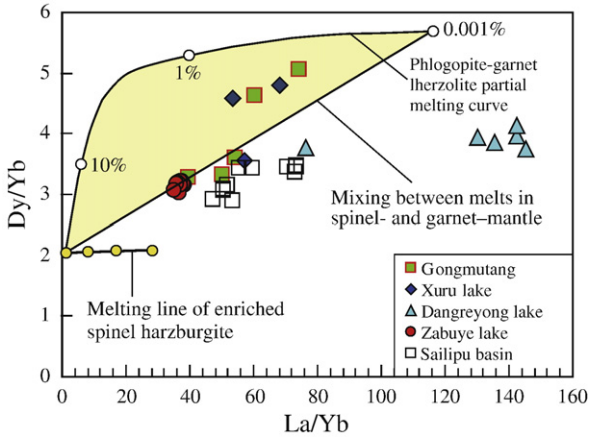

Fig. 13. Dy/Yb plotted vs. La/Yb for the ultrapotassic samples showing the rocks need an enriched mantle source for both phlogopite-bearing spinel- and garnet–mantle partial melting. All the mantle models are from Xu et al. (2001).

The extremely high incompatible element (LREE, Sr, Rb, Ba, Cs, Th, U, Pb) contents of the ultrapotassic samples indicate a two-stage enrichment process of the mantle source as suggested by Turner et al. (1993). The first stage involved the addition of a proto-Tibetan lithosphere geochemical component that produced the highly enriched lithospheric upper mantle. During this first stage the LILE and LREE contents of the mantle source would have been enhanced by 10–100 times over values in the depleted mantle. In the second stage, melts/fluids derived from the subducted Himalayan continental material added to this enriched Tibetan lithospheric mantle. During partial melting of this mantle to produce the ultrapotassic magmas, the most incompatible elements (with K_D <~0.01) were enriched another 10 to 100 times leading to total enrichments of 100–1000 times in the final ultrapotassic magmas (normalized to chondrite). If this two-stage model is correct, <1% partial melting of a phlogopite-garnet lherzolite upper mantle could generate the extremely high LILE in the lavas. For example, barium partition coefficients in basaltic rocks are commonly between 0.01 and 0.02 for olivine, clinopyroxene, orthopyroxene, and garnet (Rollinson, 1993), and thus small degrees of partial melting would increase the Ba content by least to 50–100 times over its original value. The second stage would then increase Ba from less than a hundred ppm to several thousands of ppm, as seen in the rocks described in this work (up to 5513 ppm Ba). Other incompatible elements will act in the same manner.

The ultrapotassic lavas are enriched in LILE and relatively depleted in HFSE, such as Nb, Ta, Zr, Hf, Ti, indicating subduction of Himalayan continental basement materials. Enrichment of Ba, Pb, and Sr is generally attributed to aqueous fluids, whereas partial melts of subducted sediment are thought to add Nb, Th, La, Ce, and Nd to the mantle (Kelemen et al., 2003; Castillo and Newhall, 2004). In plots of Ba, Ba/Y and Rb/Y against Nb/Y (Fig. 14), the samples from Gongmutang and Sailipu exhibit strong increases in Ba ranging from 1853 ppm to 10,170 ppm, reflecting a typical fluid-related enrichment. On the other hand, samples from Zabuye and Dangreyong lake show nearly constant Ba with increasing Nb/Y ratios, suggesting a melt-related trend. Overall, the ultrapotassic lavas from all localities in the Lhasa terrane (Fig. 14) exhibit variable Nb/Y ratios with narrow ranges of Ba (Ba/Y and Rb/Y). Thus, both melt and aqueous phases were responsible for the enrichment of the mantle source region in LILE and REE.

Additional support for melt-related enrichment of the mantle is provided by trace element data (Fig. 15). The highly variable Th/Nb ratios of the lavas indicate enrichment of the mantle by melts derived from subducted materials. The low values of Th/Nb for the ultrapotassic rocks from northern Tibet (Guo et al., 2006) may represent the initial mantle composition before enrichment occurred.

6.3. Mixing of major geochemical reservoirs in Tibet

Our Nd, Sr, Pb and O isotopic data for the ultrapotassic samples are shown in Figs. 8, 9 and 10, along with previously published data for magmatic rocks in the Lhasa terrane, northern Tibet (Qiangtang, Hoh Xil and West Kunlun), Himalayan basement and granitoids, and basaltic rocks from the Yarlung Zangbo suture. Three main geochemical reservoirs are recognized based on the Sr–Nd–Pb isotopic data and geochemistry of the post-collisional magmatic rocks across southern and northern Tibet (Mo et al., 2006a,b; Zhao et al., 2006, 2007). These three reservoirs are (Table 8 and references therein): (1) The North Tibet Geochemical Province ($^{87}Sr/^{86}Sr = 0.7071–0.7105$, $\varepsilon_{Nd} = -2$ to -8, $T_{DM} = 0.7–1.3$ Ga, $^{206}Pb/^{204}Pb = 18.662–18.996$, $^{207}Pb/^{204}Pb = 15.575–15.716$, $^{208}Pb/^{204}Pb = 38.712$ to 39.374), which has existed as a stable, homogeneous reservoir in both the crust and upper mantle since ~46 Ma. Rocks of this region have a narrow range of isotopic ratios, as revealed by the widespread shoshonitic, ultrapotassic, and adakitic rocks in the Qiangtang, Hoh Xil, and West Kunlun belts. (2) The Neo-Tethyan mantle reservoir represented by the remnant oceanic lithosphere preserved in the Yarlung Zangbo ophiolite ($^{87}Sr/^{86}Sr = 0.703–0.706$, $\varepsilon_{Nd} = +7.8$ to $+10$, $^{206}Pb/^{204}Pb = 17.707–18.164$, $^{207}Pb/^{204}Pb = 15.415–15.543$, $^{208}Pb/^{204}Pb = 37.396–38.222$), which represents an Indian plate MORB-like depleted upper mantle domain. (3) A Himalayan continental crust component represented by the basement and granitoids from the Higher and Lesser Himalayas, which have the highest Sr and lowest Nd isotopic ratios among the three reservoirs, and the oldest Nd model ages $T_{DM} = 1.9–2.9$ Ga ($\varepsilon_{Nd} = -12$ to -25), $^{87}Sr/^{86}Sr = 0.733–0.760$, or even as high as 0.90, and the average Pb isotopic ratios of the High Himalaya basement ($P^{206}Pb/^{204}Pb = 19.500–19.736$, $^{207}Pb/^{204}Pb = 15.833–15.843$ and $^{208}Pb/^{204}Pb = 40.212–40.241$). These mature continental materials located on the northern edge of the Indian continent were the first to be subducted as India collided with Asia along the Yarlung Zangbo suture.

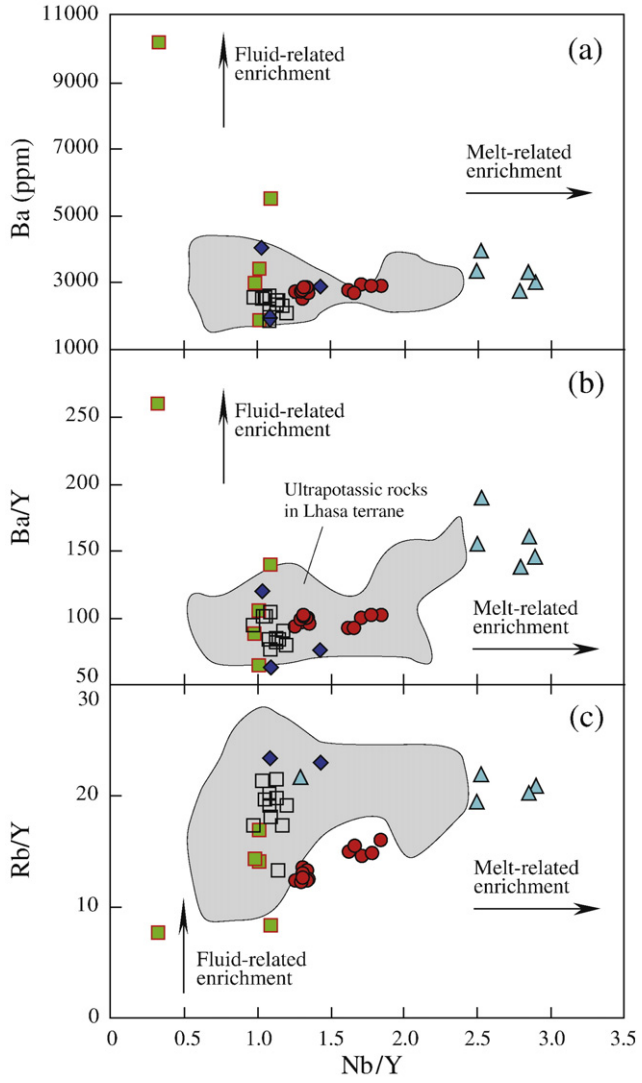

Fig. 14. Plots of Ba, Ba/Y and Rb/Y vs. Nb/Y. The samples as a whole, showing varied Nb/Y, indicate the melt-related enrichment of subducted materials. Symbols and published ultrapotassic data are as those in Fig. 4.

Three geochemical types of collisional and post-collisional magmatism are recognized in Tibet and these can be related to the proportion and degree of interaction among the three reservoirs outlined above. Each of these geochemical types has special implications for the evolution of Lhasa terrane.

The first magmatic type is inherent to the Lhasa terrane and has similar Sr–Nd compositions to those of the North Tibet Geochemical Province. These are shoshonitic rocks that crop out in Xiongba (Miller et al., 1999) and Yangying (Nomade et al., 2004). The similarity of

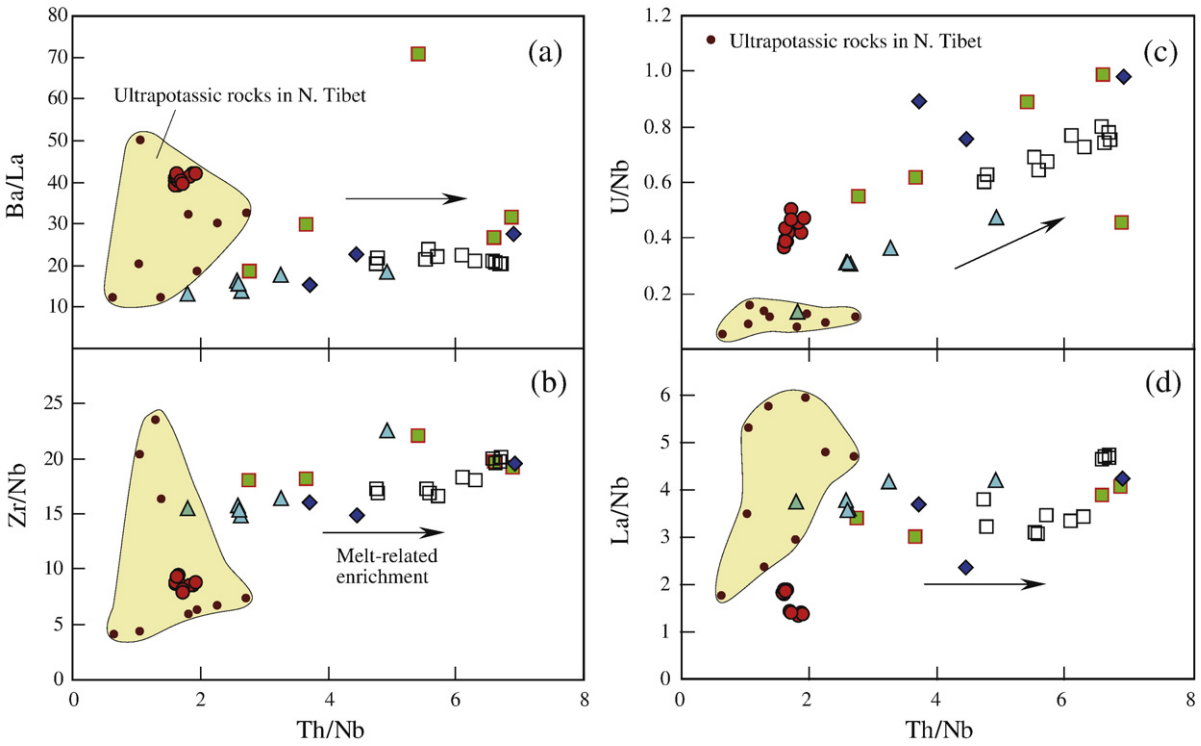

Fig. 15. Plots of Ba/La, Zr/Nb, U/Nb, and La/Nb against Th/Nb. The samples showing varied Th/Nb, indicate again the melt-related enrichment of subducted materials. Data of pure ultrapotassic samples in North Tibet (Guo et al., 2006) that match the criteria of Foley et al. (1987) are plotted for reference. Symbols are as in Fig. 4.

these rocks to those from the north Tibet suggests that the Lhasa terrane is geochemically related to the North Tibet Geochemical Province. This is supported by a similarity in He isotopes in the two terranes, all of which show a mantle origin (Hoke et al., 2000). Recently acquired geophysical data (see following sections) further support this lithospheric similarity.

The second type of magmatism, marked by a mixture of North Tibet and the Yarlung Zangbo suture end members, has Neo-Tethyan oceanic crust affinity and includes the widespread Linzizong volcanic series (44–65 Ma, Mo et al., 2003; Zhou et al., 2004; Mo et al., 2007, 2008), the I-type Gangdese granitoid batholiths (45–55 Ma, with a peak age of ~50 Ma; Mo et al., 2005; Dong et al., 2005, 2006; Wen et al., 2008), the adakitic ore-bearing porphyries (12–18 Ma; Chung et al., 2003; Hou et al., 2004; Gao et al., 2007b) and the shoshonitic rocks in the Wuyu basin (Zhao et al., 2001). These rocks, originally related to subduction and recycling of the Tethyan oceanic crust, were erupted in a later intra-plate tectonic setting following closure along the Yarlung Zangbo suture.

The third type of magmatism, represented by ultrapotassic volcanic rocks in the western Lhasa terrane, has a clear affinity to the Himalayan basement (Figs. 8–10). These rocks show a clear mixing

Table 8
Summary of Sr–Nd isotopic data from rocks in the three geochemical end-members in the Tibetan Plateau.

Rock and locality	Age (Ma)	$^{87}Sr/^{86}Sr$	ε_{Nd}	T_{DM} (Ga)	Sample numbers	Data sources
1. The North Tibet Geochemical Province						
High-K calc-alkaline, N. Qiangtang, Zuerkenwula Mt.	39–42	0.707101–0.707998	−3.1 to −5.1	0.9–1.1	17	Yi et al. (2004)
Shoshonitic, S. Qiangtang, Yulinshan	18–30	0.708766–0.709209	−7.9 to −9.2	0.9–1.3	19	Ding et al. (2003)
High-K calc-alkaline, adakitic, N. Qiangtang, Duogecuoren	38–46	0.7057–0.7097	−2.8 to −6.9	0.8–1.0	22	Wang et al. (2008a,b)
Hohxil area, K-rich adakitic volcanic rocks, Wuxuefeng, Hongshuihe, and Damaoshan	16–19	0.707211–0.707457	−2.1 to −4.4	0.7–0.8	9	Wang et al. (2005)
Potassic rocks, West Kunlun	0.1–5.6	0.707755–0.710536	−8.6 to −3.9	~0.9–1.2	37	(Turner et al., 1996; Deng, 1998; Xie, 1992; Liu, 1989; Cooper et al., 2002; Guo et al., 2006)
2. The Neo-Tethyan mantle reservoir						
Basaltic rocks in Xialu ophiolite, Xigaze	110	0.70406–0.70432	+8.2 to +9.0	–	6	Mahoney et al. (2005)
Basaltic rocks in YZS ophiolite	120–200	0.703000–0.706205	+7.8 to +9.7	–	17	Zhang et al. (2005)
Basaltic rocks in Xigaze ophiolite	110	0.703067–0.705748	+8.3 to +10.0	–	16	Niu et al. (2006)
Basaltic rocks in Yongbowa ophiolite	110	0.70300–0.703 76	+8.9 to +9.6	–	3	Miller et al. (2003)
Basaltic rocks in Xigaze ophiolite	110	0.703024–0.04681	+8.2 to +9.3	–	6	Xu and Castillo (2004)
3. Himalayan continental crust						
High Himalayan sedimentary and metamorphic rocks, granitoid	–	0.73311–0.90621	−20 to −6	1.8–2.4	Sr (63), Nd(96)	(Allègre and Ben Othman, 1980; Vidal et al., 1982, 1984; Deniel et al., 1987; Inger and Harris, 1993; Parrish and Hodges, 1996; Harrison et al., 1999; Whittington et al., 1999; Ahmad et al., 2000; Robinson et al., 2001)
Lesser Himalayan sedimentary and metamorphic rocks	–	0.7158–1.1764	−30 to −16	2.0–3.4	Sr(22), Nd(59)	
Sub-Himalaya (Siwalic) sedimentary rocks	–	–	−18 to −9	1.6–2.3	35	Robinson et al. (2001)

trend between the North Tibet Geochemical Province and the Himalayan continental crust reservoirs, thus the Sr–Nd–Pb–O data of the ultrapotassic lavas provide important evidence for subduction of the Indian continental slab beneath southern Tibet. Trace element data also support this point as mentioned above (Figs. 12a, b; 15).

We emphasize that our two-stage model for mixing between the Tibetan mantle and Himalayan basement differs from that proposed by others. During the first stage the entire Tibetan upper mantle was metasomatised by multi-stage subduction, as proposed by others (Turner et al., 1993, 1996; Ding et al., 2003; Williams et al., 2004; Guo et al., 2006). This is the dominant mantle reservoir beneath the entire Tibetan plateau, which controlled the geochemistry of the K-rich rocks in northern Tibet and parts of southern Tibet. This isolated subcontinental upper mantle is inferred to have had a long history of enrichment, based on the depleted mantle model ages (T_{DM} = 0.9 ~ 1.8 Ga) and low Nd isotope ratios of the magmas derived from this part of the mantle (>90% of the North Tibet samples have ε_{Nd} ranging from −2 to −8). In the second stage, the mantle beneath the southern part of the Tibetan Plateau was enriched by subducted continental material from the Himalayan basement.

6.4. Subduction of the Indian continent beneath southern Tibet

The pattern of subduction of the Indian continent beneath southwestern Tibet, as inferred from the Sr–Nd–Pb–O isotopic characteristics of the late Tertiary Tibetan ultrapotassic rocks along the line of Shiquanhe–Xiongba–Dangreyong lake, is of great value in delineating the present-day subduction structure between India and Asia. This line marks the junction between the Tibet mantle and the Indian continent, along which the Indian continent continues to move northward at a shallow angle. This agrees very well not only with the helium isotopic data (Hoke et al., 2000), but also with recent geophysical models (Jin et al., 1996; Kosarev et al., 1999). An important question is how far to the north has the Indian continent been subducted. A simple calculation based on the rate of northward movement of the Indian plate (40 to 50 mm/year by present GPS data; Wang et al., 2001a,b) suggests that India could have moved northward ~1200 km from the Yarlung Zangbo suture during the past 24 million years. If this calculation is correct, the northern edge of the Indian continent should now lie north of the Bangong–Nujiang suture.

However, we do not recognize any Sr–Nd–Pb isotopic evidence of a Himalayan continental crust contribution in the post-collisional rocks of northern Tibet. The isotopic characteristics of the volcanic rocks in northern Tibet have not changed over the last 46 million years, suggesting that the North Tibet Geochemical Province has not been disturbed by the India continental materials. Thus, we conclude that the Indian plate was subducted beneath southern Tibet only as far northward as the Bangong–Nujiang suture zone, at which point it plunged into the mantle. This model for subduction of the Indian continental plate is completely consistent with the existing geophysical data (Jin et al., 1996; Owens and Zandt, 1997; Kosarev et al., 1999; Chemenda et al., 2000; Wei et al., 2001; Tilmann et al., 2003; Priestley et al., 2008) and the He isotopic pattern in Tibet (Hoke et al., 2000).

One additional point concerning our subduction model for the Indian plate is that ultrapotassic rocks are currently found only west of 87°E longitude in the Lhasa terrane. If the distribution of these rocks in Tibet represents the extent of subduction of the Indian plate, the inhomogeneity between the western and eastern parts of southern Tibet suggests that India only subducted beneath the western part of the Lhasa terrane (Hou et al., 2006).

The subduction model proposed here on the basis of lava geochemistry has implications for the tectonic evolution of the Tibetan Plateau. The subduction of India beneath the Lhasa terrane would have absorbed >400 km of shortening during the convergence between India and Asia, would have thickened the crust in the Lhasa terrane by tectonic underplating, causing elevation of the Tibet Plateau, and would possibly have caused earthquakes (Barazangi and Ni, 1982; Owens and Zandt, 1997; Yin and Harrison, 2000; Johnson, 2002). This model is supported by the unconformable relationship in southern Tibet between the highly folded, upper Cretaceous Shexing Formation and the flat-lying, undisturbed rocks of the Linzizong volcanic series (Coulon et al., 1986; Yin and Harrison, 2000; Mo et al., 2003; Zhou et al., 2004; Mo et al., 2007, 2008), indicating the absence of significant Cenozoic north–south shortening in the upper crust. Geological mapping and geochronological work in a traverse across Cuoqin in the western Lhasa terrane also show that the Lhasa terrane has undergone little north–south shortening during the Cenozoic (Murphy et al., 1997).

6.5. Origin model of the ultrapotassic rocks in southern Tibet

Post-collisional ultrapotassic rocks in the Lhasa terrane provide valuable opportunities for studying the deep composition and structure of the Tibetan lithosphere and the subduction of the Indian plate beneath Asia (Beghoul et al., 1993). In Tibet, the N–S trending normal faults (or E–W extensional structures) are believed to have formed by orogenic collapse of the plateau (Molnar and Tapponnier, 1978; Dilek and Moores, 1999). The ultrapotassic rocks are regarded as evidence of mantle delamination, and are believed to indicate the time at which the plateau achieved its highest elevation, resulting in the onset of the Asian monsoon and global climate change (Williams et al., 2001). If this model is applicable to Tibet, the plateau must have gained its highest elevation before 24 Ma, because ultrapotassic magmatism began in the Lhasa terrane ~24 Ma. However, other workers argue that N–S normal faults are not related to uplift of the plateau, but rather reflect oblique convergence in which the normal faults formed by basal drag of the underthrusting Indian lithosphere (McCaffery and Nabelek, 1998). Yin et al. (1999) emphasize that the northeast-striking active faults in northern Tibet have a significant component of left-slip and suggest that the broad similarities in the magnitude of slip and the direction of extension for faults in both northern and southern Tibet imply that the entire plateau has undergone extension as part of a large-scale regional tectonic regime.

Thus, a direct link between the post-collisional magmatism and extensional tectonics has yet to be definitely established. However, we point to the fact that the post-collisional magmatism was coeval with normal faulting, dike intrusion and adakitic magmatism, as well as a series of other tectonic and magmatic events (Fig. 2b). The overlapping ages of these events imply that they were all linked to deep lithospheric process that started at ~24 Ma, either delamination (Chung et al., 2005), slab rollback (Ding et al., 2003), or slab breakoff (Mahéo et al., 2002; Kohn and Parkinson, 2002).

The post-collisional magmatism generated in the deep lithosphere was a response to continental subduction and uplift of the plateau (Harrison et al., 1992; Tapponnier et al., 2001), and hence all models for the formation of the shoshonitic and ultrapotassic rocks have to take into account the evolution of the plateau. Two different models for the origin of these rocks are currently in vogue. The first model, based largely on work in northern Tibet, suggests that the shoshonitic and ultrapotassic magmatism can be attributed to convective removal of the root of a previously thickened lithospheric mantle (England and Houseman, 1988; Arnund et al., 1992; Turner et al., 1993, 1996; Chung et al., 1998; Ding et al., 2003). This model suggests that the rocks formed in an intracontinental tectonic setting unaffected by subduction. The second model calls upon break-off/delamination of a subducted slab of Tethyan oceanic lithosphere, although the proposed timing of the break-off is disputed. Harrison et al. (1992) proposed that uplift of the plateau started at ~8 Ma as a result of delamination of the lithospheric mantle. Miller et al. (1999) noted that both of the above models are feasible but that a mechanism is needed to initiate upwelling of the asthenosphere.

In southern Tibet, the ultrapotassic rocks of Pabbai Zong west of Shigaze have been linked to thinning of the subcontinental

lithospheric mantle (Williams et al., 2001), whereas Mahéo et al. (2002) proposed that the Neogene magmatic and metamorphic evolution of the South Asian margin was controlled by slab breakoff of the subducting Indian continental margin starting at about 25 Ma. They pointed out that slab break-off would have been more efficient than the convective removal of the lithospheric mantle in southern Tibet. Kohn and Parkinson (2002) also apply a break-off model beginning at ~45 Ma to explain both the origin of the shoshonitic rocks and the exhumation of eclogite in the High Himalayan metamorphic belt. They argue that slab breakoff can easily explain the Eocene eclogites, Miocene partial melts, and late Eocene potassium-rich magmas in southeastern Tibet, and that the ages of metamorphic and plutonic events help define the timing and rates of breakoff and extrusion. Ding et al. (2003) believe that break-off of the Tethyan oceanic crust and northward underthrusting of the Indian continent have played key roles in the formation of the ultrapotassic magmatism. This model is accepted by Guo et al. (2006), who proposed that shoshonitic magmatism is a product of asthenospheric upwelling induced by the underthrusting of the Indian continent beneath Tibet.

Based on the wide spatial and temporal distribution of the potassic magmatism (Mo et al., 2006a) and earlier work (Mahéo et al., 2002; Ding et al., 2003; Chung et al., 2005), we propose a two-stage delamination model for the origin of the post-collisional magmatism within the framework of India's subduction beneath Tibet. In both stages upwelling asthenosphere is needed to generate partial melting in the upper mantle (Fig. 16). In stage 1 (~65 to 48 Ma), Linzizong Andean-type volcanic rocks were erupted in southern Tibet, whereas sparse sodic lavas were erupted farther north. The magmas were generated by dehydration melting of subducted Tethyan oceanic lithosphere. Stage 2 (~48 to 24 Ma) saw early

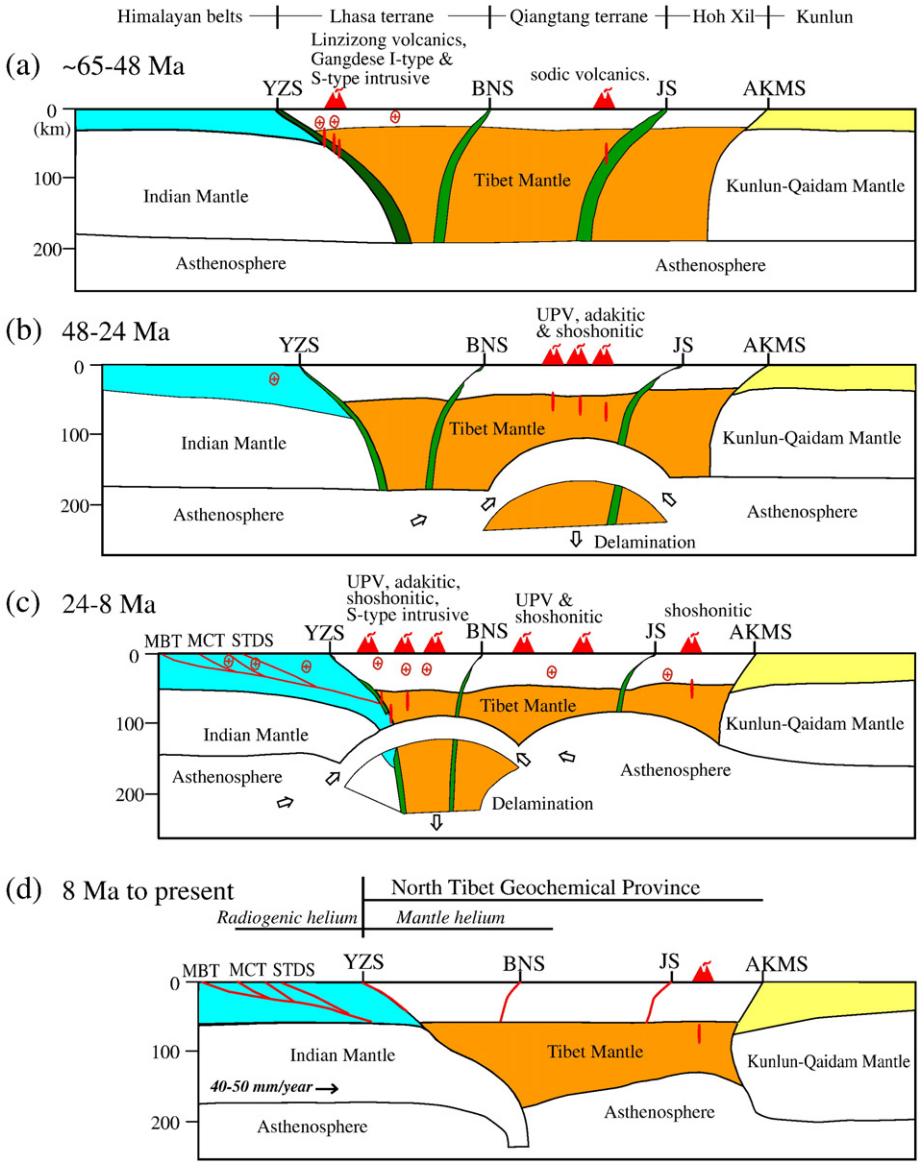

Fig. 16. Cartoon showing a genetic model for the post-collisional magmatism in the Tibetan plateau. (a) Stage 1 (~64 to 48 Ma), Tethyan oceanic lithosphere is subducted beneath South Tibet along the Yarlung Zangbo suture, and recycled in the Linzizong volcanic rocks and Gangdese batholith; (b) Stage 2 (48 to 24 Ma), the first delamination beneath the Jinsha River suture in the northern Tibet, and generation of magmatism in the north Qiangtang terrane. (c) Stage 3 (~24 to 8 Ma), the north margin of the Indian continent is subducted beneath the southwestern Lhasa block, following subduction of oceanic lithosphere. The second delamination episode in southern Tibet causes high-potassium magmatism in the Lhasa block and southern Qiangtang terrane. (d) Stage 4: 8 Ma to the present. The Indian plate continues moving northward beneath the Lhasa block and reached/passed the Bangong–Nujiang suture, terminating the heat supply of the crust and upper mantle from the upwelling asthenosphere, similar to the model proposed by Chung et al. (2005). Some mantle-derived melts formed before 10 Ma were trapped in the crust and caused the mantle helium emission in hot springs of southern Tibet (Hoke et al., 2000). Hot upper mantle and crust still exist beneath Hoh Xil, and these entities generated the youngest eruptions in the northern Tibetan Plateau. YNS, Yarlung Zangbo suture; BNS, Bangong–Nujiang suture; JS, Jinsha River suture; AKMS, Ayimaqin–Kunlun–Mutztagh suture.

delamination of southward-subducted Tethyan oceanic crust beneath the Jinsha River suture in the north Qiangtang terrane, which caused high-potassium magmatism. In the third stage (~24 to 8 Ma), subduction of the Indian continent beneath southern Tibet led to breakoff of the north-dipping slabs of both oceanic lithosphere and Indian continental material. This late delamination produced the high-potassium rocks in the Lhasa terrane, in the southern Qiangtang terrane, and in Hoh Xil. Slab detachment produced space for the progressive northward motion of the Indian continent. Our slab detachment model is close to the slab breakoff model suggested by Mahéo et al. (2002). In the final stage (~8 Ma to present), the Indian plate continued to move northward beneath the Lhasa terrane until it reached the Bangong–Nujiang suture. Emplacement of this slab terminated the transfer of heat from the upwelling asthenosphere to the crust and upper mantle, producing a magmatic gap in the Lhasa terrane. The youngest volcanic rocks, which lie just north of the Jinsha River suture, represent the latest stage of asthenospheric upwelling. However, some mantle-derived melts that formed prior to ~8 Ma were trapped in the crust, and are currently degassing mantle helium in the Lhasa terrane (Hoke et al., 2000).

7. Conclusions

Our geochemical and Sr–Nd–Pb–O isotopic data, together with previous dating, geochemical and geophysical research in the Lhasa terrane, support a genetic model involving low degrees of partial melting of an upper mantle reservoir that had undergone a two-stage metasomatic enrichment. The heat source resulted from delamination of the lower lithospheric mantle. The distinct geochemistry of the ultrapotassic rocks point to the Himalayan basement of the northern India as the most likely metasomatic agent. This interpretation implies that the Indian continent was subducted beneath southern Tibet beginning at ~24 Ma. The northern edge of the Indian continent reached the Bangong–Nujiang suture and then plunged into the upper mantle depth, an interpretation which is consistent with the present geophysical structure of the India–Asia collision in southern Tibet.

Acknowledgments

This work was supported by the National Key Project for Basic Research (2009CB421002, 2002CB412600), NSF of China (Nos. 40873023, 40830317, 40473020, 40672044, 40503005, 40572048), 111 project (B07011), China Geological Survey and China Scholarship Council projects to authors in China; and NSF grants to Y.D., D.J.D in the United States and an NSERC grant to PTR in Canada. Tom Owens and Lisa Hamersley are thanked for their help during Sr–Nd analysis at UC Berkeley, and O analysis in LBNL. We thank Zhengfu Guo and one anonymous reviewer together with Lithos Editor-in-Chief Andrew Kerr and journal manager Ruud Koole for helpful comments that improved the manuscript.

Appendix A. Supplementary data

Supplementary data associated with this article can be found, in the online version, at doi:10.1016/j.lithos.2009.02.004.

References

Ahmad, T., Harris, N., Bickle, M., Chapman, H., Bunbury, J., Prince, C., 2000. Isotopic constraints on the structural relationships between the Lesser Himalayan Series and the High Himalayan Crystalline Series, Garhwal Himalaya. Geological Society of America Bulletin 112, 467–477.

Allègre, C.J., Ben Othman, D., 1980. Nd–Sr isotopic relationships in granitoid rocks and continental crust development: a chemical approach to orogenesis. Nature 286, 335–342.

Argand, E., 1924. La tectonique de l' Asie. Proc. 13th International Geological Congress, vol. 7, pp. 171–372.

Arnund, N.O., Vidal, Ph., Tapponnier, P., Matte, Ph., Deng, W.M., 1992. The high K2O volcanism of northwestern Tibet: geochemistry and tectonic implications. Earth Planetary Science Letters 111, 351–367.

Barazangi, M., Ni, J., 1982. Velocities and propagation characteristic of Pn and Sn beneath the Himalaya arc and Tibetan plateau: possible evidence for underthrusting of Indian continental lithosphere beneath Tibet. Geology 10, 179–185.

Battistini, G.D., Montanini, A., Vernia, L., Venturelli, G., Tonarini, S., 2001. Petrology of melilite-bearing rocks from the Montefiascone Volcanic Complex (Roman Magmatic Province): new insights into the ultrapotassic volcanism of Central Italy. Lithos 59, 1–24.

Beghoul, N., Barazangi, M., Isacks, B.L., 1993. Lithospheric structure of Tibet and Western North America: mechanisms of uplift and a comparative study. Journal of Geophysical Research 98, 1997–2016.

Blattner, P., Dietrich, V., Gansser, A., 1983. Contrasting ^{18}O-enrichment and origins of High Himalayan and Transhimalayan intrusives. Earth and Planetary Science Letters 65, 276–286.

Blattner, P., Jin, C.-w., Xu, Y., 1989. Oxygen isotopes in mantle related and geothermally altered magmatites of the Transhimalayan (Gangdese) ranges. Contributions to Mineralogy and Petrology 101, 438–446.

Blattner, P., Abart, R., Adams, C.J., Faure, K., Hui, L., 2002. Oxygen isotope trends and anomalies in granitoids of the Tibetan plateau. Journal of Asian Earth Sciences 21, 241–250.

Blisniuk, P.M., Hacker, B., Glodny, J., Ratschbacher, L., Bill, S., Wu, Z.-H., McWilliams, M.O., Calvert, A., 2001. Normal faulting in central Tibet since at least 13.5 Myr ago. Nature 412, 628–632.

Boynton, W.V., 1984. Geochemistry of the rare earth elements: meteorite studies. In: Henderson, P. (Ed.), Rare Earth Element Geochemistry. Elsevier, pp. 63–114.

Castillo, P.R., Newhall, C.G., 2004. Geochemical constraints on possible subduction components in lavas of Mayon and Taal volcanoes, southern Luzon, Philippines. Journal of Petrology 45, 1089–1108.

Chemenda, A.I., Burg, J.-P., Mattauer, M., 2000. Evolutionary model of the Himalaya–Tibet system: geopoem based on new modelling, geological and geophysical data. Earth and Planetary Science Letters 174, 397–409.

Chen, W.-P., Ozalaybey, S., 1998. Correlation between seismic anisotropy and Bouguer gravity anomalies in Tibet and its implications for lithospheric structures. Geophysical Journal International 135, 93–101.

Chen, J.L., Xu, J.F., Kang, Z.Q., Wang, B.D., 2006. Origin of the Miocene Bugasi group volcanic rocks in the Cuoqin County, western Tibetan plateau. Acta Petrologica Sinica 22, 585–594 (in Chinese, with English abstract).

Chung, S.-L., Lo, C.-H., Lee, T.-Y., Zhang, Y., Xie, Y., Li, X., Wang, K.-L., Wang, P.-L., 1998. Diachronous uplift of the Tibetan Plateau starting 40 Myr ago. Nature 394, 769–773.

Chung, S.-L., Liu, D., Ji, J., Chu, M.-F., Lee, H.-Y., Wen, D.-J., Lo, C.-H., Lee, T.-Y., Qian, Q., Zhang, Q., 2003. Adakite from continental collision zones: melting of thickened lower crust beneath southern Tibet. Geology 31, 1021–1024.

Chung, S.-L., Chu, M.-F., Zhang, Y., Xie, Y., Lo, C.-H., Lee, T.-Y., Lan, C.-Y., Li, X., Zhang, Y.Q., Wang, Y., 2005. Tibetan tectonic evolution inferred from spatial and temporal variations in post-collisional magmatism. Earth Science Reviews 68, 173–196.

Clayton, R.N., Mayeda, T.K., 1963. The use of bromine pentafluoride in the extraction of oxygen from oxides and silicates for isotopic analysis. Geochimica et Cosmochimica Acta 27, 43–52.

Coleman, M., Hodges, K., 1995. Evidence for Tibetan plateau uplift before 14 Myr ago from a new minimum age for east–west extension. Nature 374, 49–52.

Conticelli, S., 1998. The effect of crustal contamination on ultrapotassic magmas with lamproitic affinity: mineralogical, geochemical and isotope data from the Torre Alfina lavas and xenoliths, Central Italy. Chemical Geology 149, 51–81.

Conticelli, S., Peccerillo, A., 1992. Petrology and geochemistry of potassic and ultrapotassic volcanism in central Italy: petrogenesis and inferences on the evolution of the mantle sources. Lithos 28, 221–240.

Conticelli, S., D'Antonio, M., Pinarelli, L., Civetta, L., 2002. Source contamination and mantle heterogeneity in the genesis of Italian potassic and ultrapotassic volcanic rocks: Sr–Nd–Pb isotope data from Roman Province and Southern Tuscany. Mineralogy and Petrology 74, 189–222.

Conticelli, S., Marchionni, S., Rosa, D., Giordano, G., Boari, E., Avanzinelli, R., 2009. Shoshonite and sub-alkaline magmas from an ultrapotassic volcano: Sr–Nd–Pb isotope data on the Roccamonfina volcanic rocks, Roman Magmatic Province, Southern Italy. Contributions to Mineralogy and Petrology 157, 41–63.

Cooper, K.M., Reid, M.R., Dunbar, N.W., McIntosh, W.C., 2002. Origin of mafic magmas beneath northwestern Tibet: constraints from ^{230}Th–^{238}U disequilibria. Geochemistry, Geophysics, Geosystems (G-cubed) 3 (1). doi:10.1029/2002GC000332.

Copeland, P.H., Harrison, T.M., Kidd, W.S.F., Xu, R.-H., Zhang, Y.-Q., 1987. Rapid early Miocene acceleration of uplift in the Gangdese belt, Xizang (south Tibet) and its bearing on accommodation mechanism of the India–Asia collision. Earth and Planetary Science Letters 86, 240–252.

Corriveau, L., 1990. Proterozoic subduction and terrane amalgamation in the south-western Grenville province, Canada: evidence from ultrapotassic to shoshonitic plutonism. Geology 15, 614–617.

Coulon, C., Maluski, H., Bollinger, C., Wang, S., 1986. Mesozoic and Cenozoic volcanic rocks from central and southern Tibet: ^{39}Ar–^{40}Ar dating, petrological characteristics and geodynamical significance. Earth and Planetary Science Letters 79, 281–302.

Da Silva Filho, A.F., Guimaraes, I.P., Thompson, R.N., 1993. Shoshonitic and ultrapotassic Proterozoic intrusive suites in the Cachoeirinha–Salgueiro belt, NE Brazil: a transition from collisional to post-collisional Magmatism. Precambrian Research 62, 323–342.

Davis, L.L., Smith, D., McDowell, F.W., Walker, N.W., Borg, L.E., 1996. Eocene potassic Magmatism at Two Buttes, Colorado, with implications for Cenozoic tectonics and magma generation in the western United States. Geological Society of America Bulletin 108, 1567–1579.

Debon, F., Le Fort, P., Sheppard, S.M.F., Sonet, J., 1986. The four plutonic belts of the Transhimalaya–Himalaya: a chemical, mineralogical, isotopic and chronological synthesis along a Tibet–Nepal section. Journal of Petrology 27, 281–302.

Defant, M.J., Xu, J.F., Kepezhinskas, P., Wang, Q., Zhang, Q., Xiao, L., 2002. Adakites: some variations on a theme. Acta Petrological Sinica 18, 129–142.
Deng, W., 1998. Cenozoic Intraplate Volcanic Rocks in the Northern Qinghai–Xizang Plateau. Geological Publishing House, Beijing.
Deniel, C., Vidal, P., Fernandez, A., Le Fort, P., Peucat, J.-J., 1987. Isotopic study of the Manaslu granite (Himalaya, Nepal): inferences on the age and source of Himalayan leucogranites. Contributions to Mineralogy and Petrology 96, 78–92.
DePaolo, D.J., Daley, E.E., 2000. Neodymium isotopes in basalts of the southwest basin and range and lithospheric thinning during continental extension. Chemical Geology 169, 157–185.
Dewey, J.F., Shackleton, R.M., Chang, C., Sun, Y., 1988. The tectonic evolution of the Tibetan plateau. Philosophical Transactions of the Royal Society, London A327, 379–413.
Dilek, Y., Altunkaynak, S., 2007. Cenozoic crustal evolution and mantle dynamics of post-collisional magmatism in western Anatolia. International Geology Review 49, 431–453. doi:10.2747/0020-6814.49.5.431.
Dilek, Y., Altunkaynak, S., 2008. Geochemical and temporal evolution of Cenozoic magmatism in western Turkey: Mantle response to collision, slab breakoff, and lithospheric tearing in an orogenic belt. In: Van Hinsbergen, D.J.J., Edwards, M.A., Govers, R. (Eds.), Collision and Collapse at the Africa–Arabia–Eurasia Subduction Zone. Geological Society of London Special Publications, vol. 311, pp. 213–233. doi:10.1144/SP311.8.
Dilek, Y., Moores, E.M., 1999. A Tibetan model for the Early Tertiary western United States. Journal of the Geological Society of London 156, 929–942. doi:10.1144/gsjgs.156.5.0929.
Ding, L., Zhang, J., Zhou, Y., Deng, W., Xu, R., Zhong, D., 1999. Tectonic implication on the lithosphere evolution of the Tibetan Plateau: petrology and geochemistry of sodic and ultrapotassic volcanism in Northern Tibet. Acta Petrologica Sinica 15, 408–421 (in Chinese, with English abstract).
Ding, L., Kapp, P., Zhong, D., Deng, W., 2003. Cenozoic volcanism in Tibet: evidence for a transition from oceanic to continental subduction. Journal of Petrology 44, 1833–1865.
Ding, L., Yue, Y., Cai, F., Xu, X., Zhang, Q., Lai, Q., 2006. $^{40}Ar/^{39}Ar$ geochronology, geochemical and Sr–Nd–O isotopic characteristics of the high-Mg ultrapotassic rocks in Lhasa block of Tibet: implications in the onset time and depth of NS-striking rift system. Acta Geologica Sinica 80, 1252–1261 (in Chinese, with English abstract).
Dong, G.C., Mo, X.X., Zhao, Z., Guo, T., Wang, L.L., Chen, T., 2005. Geochronologic constraints by SHRIMP II zircon U–Pb dating on magma underplating in the Gangdise belt following India–Eurasia collision. Acta Geologica Sinica 79, 787–794.
Dong, G.C., Mo, X.X., Zhao, Z., Zhu, D.C., Wang, L.L., Chen, T., Li, B., 2006. Magma mixing in the middle part of the Gangdise magmatic belt: evidence from granitoid complexes. Acta Petrologica Sinica 24, 835–844.
Elburg, M., Kamenetsky, V.S., 2008. Limited influence of subducted continental material on mineralogy and elemental geochemistry of primitive magmas from Indonesia–Australia collision zone. Lithos 105, 73–84. doi:10.1016/j.lithos.2008.02.010.
England, P.C., Houseman, G., 1986. Finite strain calculations of continental deformation 2. Comparison with the India–Asia collision zone. Journal of Geophysical Research 91, 3664–3676.
England, P.C., Houseman, G., 1988. The mechanics of the Tibetan plateau. Philosophical Transactions of the Royal Society, London A326, 301–319.
England, P.C., Houseman, G., 1989. Extension during continental convergence, with application to the Tibetan plateau. Journal of Geophysical Research 94, 17561–17579.
Foley, S.F., Venturelli, G., Green, D.H., Toscani, L., 1987. The ultrapotassic rocks: characteristics, classification and constraints for petrogenetic models. Earth Science Reviews 24, 81–134.
France-Lanord, C., Sheppard, S.M.F., Le Fort, P., 1988. Hydrogen and oxygen isotope variations in the Higher Himalaya peraluminous Manaslu leucogranite: evidence for heterogeneous sedimentary source. Geochemica et Cosmochimica Acta 52, 513–526.
Gao, Y., Hou, Z., Kamber, B.S., Wei, R., Meng, X., Zhao, R., 2007a. Lamproitic rocks from a continental collision zone: evidence for recycling of subducted Tethyan oceanic sediments in the mantle beneath Southern Tibet. Journal of Petrology 48, 729–752.
Gao, Y., Hou, Z., Kamber, B.S., Wei, R., Meng, X., Zhao, R., 2007b. Adakite-like porphyries from the southern Tibetan continental collision zones: evidence for slab melt metasomatism. Contributions to Mineralogy and Petrology 153, 105–120.
Gao, S., Rudnick, R.L., Xu, W.L., Yuan, H.L., Liu, Y.S., Walker, R.J., Puchtel, I.S., Liu, X.M., Huang, H., Wang, X.R., Yang, J., 2008. Recycling deep cratonic lithosphere and generation of intraplate magmatism in the North China Craton. Earth and Planetary Science Letters 270, 41–53.
Guo, Z., Wilson, M., Liu, J., Mao, Q., 2006. Post-collisional, potassic and ultrapotassic magmatism of the Northern Tibetan Plateau: constraints on characteristics of the mantle source, geodynamic setting and uplift mechanisms. Journal of Petrology 47, 1177–1220.
Guo, Z., Wilson, M., Liu, J., 2007. Post-collisional adakites in south Tibet: products of partial melting of subduction-modified lower crust. Lithos 96, 205–224.
Guynn, J.H., Kapp, P., Pullen, A., Heizler, M., Gehrels, G., Ding, L., 2006. Tibetan basement rocks near Amdo reveal "missing" Mesozoic tectonism along the Bangong suture, central Tibet. Geology 34, 505–508.
Harris, N.B.W., Xu, R., Lewis, C.L., Hawkesworth, C.J., Zhang, Y., 1988. Isotope geochemistry of the 1985 Tibet Geotraverse, Lhasa to Golmud. Philosophical Transactions of the Royal Society of London, Series A327, 263–285.
Harrison, T.M., Copeland, P., Kidd, W.S.F., Yin, A., 1992. Raising Tibet. Science 255, 1663–1670.
Harrison, T.M., Grove, M., McKeegan, K.D., Coath, C.D., Lovera, O.M., Le Fort, P., 1999. Origin and episodic emplacement of the Manaslu intrusive complex, Central Himalaya. Journal of Petrology 40, 3–19.
Hoke, L., Lamb, S., Hilton, D.R., Poreda, R.J., 2000. Southern limit of mantle-derived geothermal helium emissions in Tibet: implications for lithospheric structure. Earth and Planetary Science Letters 180, 297–308.
Hou, Z.Q., Gao, Y.F., Qu, X.M., Rui, Z.Y., Mo, X.X., 2004. Origin of adakitic intrusives generated during mid-Miocene east–west extension in southern Tibet. Earth and Planetary Science Letters 220, 139–155.
Hou, Z.Q., Zhao, Z.D., Gao, Y.F., Yang, Z.M., Jiang, W., 2006. Tearing and diachronous subduction of the Indian continental slab: evidence from Cenozoic Gangdese volcano-magmatic rocks in southern Tibet. Acta Geologica Sinica 22, 761–774 (in Chinese, with English Abstract).
Houseman, G.A., McKenzie, D.P., Molnar, P., 1981. Convective instability of a thickened boundary layer and its relevance for the thermal evolution of continental convergent belts. Journal of Geophysical Research 86, 6115–6132.
Inger, S., Harris, N., 1993. Geochemical constraints on leucogranite magmatism in the Langtang Valley, Nepal Himalaya. Journal of Petrology 34, 345–368.
Jiang, W., Mo, X.X., Zhao, C.H., Guo T.Y., Zhang, S.Q., 1999. Geochemistry of granitoid and its mafic microgranular enclave in Gangdise belt, Qinghai-Xizang Plateau. Acta Petrologica Sinica 15, 89–97 (in Chinese, with English abstract).
Jin, Y., McNutt, M.K., Zhu, Y., 1996. Mapping the descent of Indian and Eurasian plates beneath the Tibetan Plateau from gravity anomalies. Journal of Geophysical Research 101, 11275–11290.
Johnson, M.R.W., 2002. Shortening budgets and role of continental subduction during the India–Asia collision. Earth Science Reviews 59, 101–123.
Kelemen, P.B., Hanghøj, K., Greene, A.R., 2003. One view of the geochemistry of subduction-related magmatic arcs, with an emphasis on primitive andesite and lower crust. In: The Crust (ed. R.L., Rudnick) vol. 3. Treatise on Geochemistry (eds. H.D., Holland and K.K., Turekian). Elsevier-Pergamon, Oxford. pp. 593–659.
Kind, R., Yuan, X., Saul, J., Nelson, D., Sobolev, S.V., Mechie, J., Zhao, W., Kosarev, G., Ni, J., Achauer, U., Jiang, M., 2002. Seismic images of crust and upper mantle beneath Tibet: Evidence for Eurasian plate subduction. Science 298, 1219–1221.
Kohn, M.J., Parkinson, C.D., 2002. Petrologic case for Eocene slab breakoff during the Indo-Asian collision. Geology 30, 591–594.
Kosarev, G., Kind, R., Sobolev, S.V., Yuan, X., Hanka, W., Oreshin, S., 1999. Seismic evidence for a detached Indian lithosphere mantle beneath Tibet. Science 283, 1306–1309.
Le Maitre, R.W., 1989. A classification of Igneous Rock and Glossary of Terms. Blackwell Science Publication, Oxford.
Liao, S., Chen, Z., Luo, X., Zou, A., 2002. Discovery of leucite phonolite in the Tangra Yumco area, Tibet and its geological significance. Geological Bulletin of China 21, 735–738 (in Chinese, with English Abstract).
Liu, J., 1989. Comment on 'ages and distributions of the volcanic rocks in Pulu, Xinjing, China'. Acta Petrologica Sinica 2, 95–97 (in Chinese with English abstract).
Ma, R., Liu, D., Tao, X., Shi, H., Hu, X., 2002. Discovery of Tertiary potassium-rich magmatic rocks in the Coqen area, Tibet. Geological Bulletin of China 21, 728–731 (in Chinese, with English abstract).
Mahéo, G., Guillot, S., Blichert-Toft, J., Rolland, Y., Pêcher, A., 2002. A slab breakoff model for the Neogene thermal evolution of south Karakorum and south Tibet. Earth and Planetary Science Letters 195, 45–58.
Mahoney, J.J., Frei, R., Tejada, M.L.G., Mo, X.X., Leat, P.T., Nagler, T.F., 2005. Tracing the Indian Ocean mantle domain through time: isotopic results from old West Indian, East Tethyan, and South Pacific seafloor. Journal of Petrology 39, 1285–1306.
McCaffery, R., Nabelek, J., 1998. Role of oblique convergence in the active deformation of the Himalaya and southern Tibet plateau. Geology 26, 691–694.
Miller, C., Schuster, R., Klotzli, U., Frank, W., Grasemann, B., 1999. Post-collisional potassic and ultrapotassic magmatism in SW Tibet: geochemical and Sr–Nd–Pb–O isotopic constraints for mantle source characteristics and petrogenesis. Journal of Petrology 40, 1399–1424.
Miller, C., Thöni, M., Frank, W., Schuster, R., Melcher, F., Meisel, T., Zanetti, A., 2003. Geochemistry and tectonomagmatic affinity of the Yungbwa ophiolite, SW Tibet. Lithos 66, 155–172.
Mo, X., Zhao, Z., Deng, J., Dong, G., Zhou, S., Guo, T., Zhang, S., Wang, L., 2003. Response of volcanism to the India–Asia collision. Earth Science Frontiers 10, 135–148 (in Chinese, with English abstract).
Mo, X., Dong, G., Zhao, Z., Guo, T., Wang, L., Chen, T., 2005. Timing of magma mixing in the Gangdise magmatic belt during the India–Asia collision: zircon SHRIMP U–Pb dating. Acta Geologica Sinica 79, 66–76.
Mo, X., Zhao, Z., Deng, J., Flower, M., Yu, X., Luo, Z., Li, Y., Zhou, S., Dong, G., Zhu, D., Wang, L., 2006a. Petrology and geochemistry of postcollisional volcanic rocks from the Tibetan plateau: implications for lithosphere heterogeneity and collision-induced asthenospheric mantle flow. In: Dilek, Y., Pavlides, S. (Eds.), Postcollisional Tectonics and Magmatism in the Mediterranean Region and Asia. Geological Society of America Special Paper, vol. 409, pp. 507–530. doi:10.1130/2006.2409(24).
Mo, X.X., Zhao, Z.D., DePaolo, D.J., Zhou, S., Dong, G.C., 2006b. Three types of collisional and post-collisional magmatism in the Lhasa block, Tibet and implications for India continental subduction and mineralization: evidence from Sr–Nd isotopes. Acta Petrologica Sinica 22, 795–803.
Mo, X., Hou, Z., Niu, Y., Dong, G., Qu, X., Zhao, Z., Yang, Z., 2007. Mantle contributions to crustal thickening during continental collision: evidence from Cenozoic igneous rocks in southern Tibet. Lithos 96, 225–242.
Mo, X., Niu, Y., Dong, G., Zhao, Z., Hou, Z., Zhou, S., Ke, S., 2008. Contribution of syncollisional felsic magmatism to continental crust growth: a case study of the Paleogene Linzizong volcanic succession in southern Tibet. Chemical Geology 250, 49–68.
Molnar, P., Tapponnier, P., 1975. Cenozoic tectonics of Asia: effects of a continental collision. Science 189, 419–426.
Molnar, P., Tapponnier, P., 1978. Active tectonics of Tibet. Journal of Geophysical Research 85, 5361–5375.

Morimoto, N., 1988. Nomenclature of pyroxenes. Mineralogy and Petrology 39, 55–76.
Müller, D., Groves, D.I., 2000. Potassic Igneous Rocks and Associated Gold–Copper Mineralization. Springer, p. 252.
Murphy, M.A., Yin, A., Harrison, T.M., Dürr, S.B., Chen, Z., Ryerson, F.J., Kidd, W.S.F., Wang, X., Zhou, X., 1997. Did the Indo-Asian collision alone create the Tibetan plateau? Geology 25, 719–722.
Niu, X.L., Zhao, Z.D., Mo, X.X., DePaolo, D.J., Dong, G.C., Zhang, S.Q., Zhu, D.C., Guo, T.Y., 2006. Elemental and Sr–Nd–Pb isotopic geochemistry for basic rocks from Decun–Angren ophiolites in the Xigaze area, Tibet: implications for the characteristics of the Tethyan upper mantle domain. Acta Petrologica Sinica 22, 2875–2888.
Nomade, S., Renne, P.R., Mo, X., Zhao, Z., Zhou, S., 2004. Miocene volcanism in the Lhasa block: spatial trends and geodynamic implications. Earth and Planetary Science Letters 221, 227–243.
Owens, T.J., Zandt, G., 1997. Implications of crustal property variations for models of Tibetan plateau evolution. Nature 387, 37–43.
Parrish, R.R., Hodges, K.V., 1996. Isotopic constraints on the age and provenance of the Lesser and Greater Himalayan sequences, Nepalese Himalaya. Geological Society of America Bulletin 108, 467–477.
Pêcher, A., Bouchez, J.-L., Le Fort, P., 1991. Miocene dextral shearing between Himalaya and Tibet. Geology 19, 683–685.
Plank, T., Langmuir, C.H., 1998. The chemical composition of subducting sediment and its consequences for the crust and mantle. Chemical Geology 145, 325–394.
Powell, C.M., Conaghan, P.J., 1973. Plate tectonics and the Himalaya. Earth and Planetary Science Letters 20, 1–12.
Priestley, K., Jackson, J., McKenzie, D., 2008. Lithospheric structure and deep earthquakes beneath India, the Himalaya and southern Tibet. Geophysical Journal International 172, 345–362.
Robinson, D.M., DeCelles, P.G., Patchett, P.J., Garzione, C.N., 2001. The kinematic evolution of the Nepalese Himalaya interpreted from Nd isotopes. Earth and Planetary Science Letters 192, 507–521.
Rollinson, H.R., 1993. Geochemical Data: Evaluation, Presentation and Interpretation. John Wiley & Sons, Inc, New York, pp. 104–133.
Rudnick, R., Gao, S., 2003. Composition of the continental crust, In: The crust (ed. R.L., Rudnick) vol.3. Treatise on Geochemistry (eds. H.D., Holland and K.K., Turekian). Elsevier-Pergamon, Oxford, pp.1–64.
Rudnick, R.L., Gao, S., Ling, W.L., Liu, Y.S., McDonough, W.F., 2004. Petrology and geochemistry of spinel peridotite xenoliths from Hannuoba and Qixia, North China Craton. Lithos 77, 609–637.
Sheppard, S., Taylor, W.R., 1992. Barium- and LREE-rich, olivine–mica–lamprophyres with affinities to lamproites, Mt. Bundey, Northern Territory, Australia. Lithos 28, 303–325.
Smith, J.V., 1974. Feldspar Minerals. Crystal Structure and Physical Properties, vol. 1. Springer-Verlag, Berlin. 318 p.
Spicer, R.A., Harris, N.B.W., Widdowson, M., Herman, A.B., Guo, S., Valdes, P.J., Wolfek, J.A., Kelley, S.P., 2003. Constant elevation of southern Tibet over the past 15 million years. Nature 421, 622–624.
Sun, S., McDonough, W.F., 1989. Chemical and isotopic systematics of oceanic basalts: implications for mantle composition and processes. In: Saunders, A.D., Norry, M.J. (Eds.), Magmatism in the Ocean Basins. Geological Society London. Special Publications, vol. 42, pp. 313–345.
Sun, C.G., Zhao, Z.D., Mo, X.X., Zhu, D.C., Dong, G.C., Zhou, S., Dong, X., Xie, G.G., 2007. Geochemistry and origin of the Miocene Sailipu ultrapotassic rocks on western Lhasa block, Tibetan Plateau. Acta Petrologica Sinica 23, 2715–2726 (in Chinese, with English abstract).
Sun, C.G., Zhao, Z.D., Mo, X.X., Zhu, D.C., Dong, G.C., Zhou, S., Chen, H.H., Xie, L.W., Yang, Y.H., Sun, J.F., Yu, F., 2008. Enriched mantle source and petrogenesis of Sailipu ultrapotassic rocks in southwestern Tibetan Plateau: constraints from zircon U–Pb geochronology and Hf isotopic compositions. Acta Petrologica Sinica 24, 249–264 (in Chinese, with English abstract).
Tapponnier, P., Xu, Z., Rogers, F., Meyer, B., Arnaud, N., Wittlinger, G., Yang, J., 2001. Oblique stepwise rise and growth of the Tibet plateau. Science 294, 1671–1677.
Thompson, R.N., Gibson, S.A., 2000. Transient high temperatures in mantle plume heads inferred from magnesian olivines in Phanerozoic picrites. Nature 407, 502–506.
Tilmann, F., Ni, J., INDEPTH III Seismic Team, 2003. Seismic imaging of the downwelling Indian lithosphere beneath Central Tibet. Science 300, 1424–1427.
Turner, S., Hawkesworth, C., Liu, Rogers, N., Kelley, S., van Calsteren, P., 1993. Timing of Tibetan uplift constrained by analysis of volcanic rocks. Nature 364, 50–54.
Turner, S., Arnaud, N., Liu, J., Rogers, N., Hawkesworth, C., Harris, N., Kelley, S., 1996. Post-collision, shoshonitic volcanism on the Tibetan Plateau: Implications for convective thinning of the lithosphere and the source of ocean island basalts. Journal of Petrology 37, 45–71.
Vidal, Ph., Cocherie, A., Le Fort, P., 1982. Geochemical investigations of the origin of the Manaslu leucogranite (Himalaya, Nepal). Geochimica et Cosmochimica Acta 46, 2279–2292.
Vidal, Ph., Bernard-Griffiths, J., Cocherie, A., 1984. Geochemical comparison between Himalayan and Hercynian leucogranites. Physics of the Earth and Planetary Interiors 35, 179–190.
Wang, J.-H., Yin, A., Harrison, T.M., Grove, M., Zhang, Y.-Q., Xie, G.-H., 2001a. A tectonic model for Cenozoic igneous activities in the eastern Indo-Asian collision zone. Earth and Planetary Science Letters 188, 123–133.
Wang, Q., Zhang, P.-Z., Freymueller, J.T., Bilham, R., Larson, K.M., Lai, X., You, X., Niu, Z., Wu, J., Li, Y., Liu, J., Yang, Z., Chen, Q., 2001b. Present-day crustal deformation in China constrained by global positioning system measurements. Science 294, 574–577.
Wang, Q., McDermott, F., Xu, J.F., Bellon, H., Zhu, Y.T., 2005. Cenozoic K-rich adakitic volcanic rocks in the Hohxil area, northern Tibet: lower-crustal melting in an intracontinental setting. Geology 33, 465–468.
Wang, B.D., Xu, J.F., Zhang, X.G., Chen, J.L., Kang, Z.Q., Dong, Y.H., 2008a. Petrogenesis of Miocene volcanic rocks in the Sailipu area, Western Tibetan Plateau: geochemical and Sr–Nd isotopic constraints. Acta Petrologica Sinica 24, 265–278 (in Chinese, with English abstract).
Wang, Q., Wyman, D.A., Xu, J., Dong, Y., Vasconcelos, P.M., Pearson, N., Wan, Y., Dong, H., Li, C., Yu, Y., Zhu, T., Feng, X., Zhang, Q., Zi, F., Chu, Z., 2008b. Eocene melting of subducting continental crust and early uplifting of central Tibet: evidence from central-western Qiangtang high-K calc-alkaline andesites, dacites and rhyolites. Earth and Planetary Science Letters 272, 158–171.
Wei, W., Unsworth, M., Jones, A., Booker, J., Tan, H., Nelson, D., Chen, L., Li, S., Solon, K., Bedrosian, P., Jin, S., Deng, M., Ledo, J., Kay, D., Roberts, B., 2001. Detection of widespread fluids in the Tibetan crust by magnetotelluric studies. Science 292, 716–718.
Wen, D.-R., Chung, S.-L., Song, B., Iizuka, Y., Yang, H.-J., Ji, J., Liu, D., Gallet, S., 2008. Late Cretaceous Gangdese intrusions of adakitic geochemical characteristics, SE Tibet: petrogenesis and tectonic implications. Lithos 105, 1–11. doi:10.1016/j.lithos.2008.02.005.
Whittington, A., Foster, G., Harris, N., 1999. Lithostratigraphic correlations in the western Himalaya— an isotopic approach. Geology 7, 585–588.
Willett, S.D., Beaumont, C., 1994. Subduction of Asian lithospheric mantle beneath Tibet inferred from models of continental collision. Nature 369, 642–645.
Williams, H., Turner, S., Kelley, S., Harris, N., 2001. Age and composition of dikes in Southern Tibet: new constraints on the timing of east–west extension and its relationship to postcollisional volcanism. Geology 29, 339–342.
Williams, H.M., Turner, S.P., Pearce, J.A., Kelley, S.P., Harris, N.B.W., 2004. Nature of the source regions for post-collisional, potassic magmatism in southern and northern Tibet from geochemical variations and inverse trace element modelling. Journal of Petrology 45, 555–607.
Wilson, M., 2001. Igneous Petrogenesis. Unwin Hyman, London.
Xie, G., 1992. Geochemistry of the Cenozoic volcanic rocks in the margins of Tibetan Plateau: evidence for an ancient enriched mantle. In: Liu, R. (Ed.), Geochronology and Geochemistry of Cenozoic Volcanic Rock in China. Seismology Press Beijing, pp. 400–427.
Xu, J.F., Castillo, P.R., 2004. Geochemical and Nd–Pb isotopic characteristics of the Tethyan asthenosphere: implications for the origin of the Indian Ocean mantle domain. Tectonophysics 393, 9–27.
Xu, Y.-G., Menzies, M.A., Thirlwall, M.F., Xie, G.H., 2001. Exotic lithosphere mantle beneath the western Yangtze craton: petrogenetic links to Tibet using highly magnesian ultrapotassic rocks. Geology 29, 863–866.
Yang, J.S., Wu, C.L., Shi, R.D., Li, H.B., Xu, Z.Q., Meng, F.C., 2002. Miocene and Pleistocene shoshonitic volcanic rocks in the Jingyuhu area, northern part of the Qinghai–Tibet Plateau. Acta Petrologica Sinica 18, 161–176.
Yi, H., Lin, J., Li, B., 2004. Cenozoic High-Potassic Calc-Alkaline Series Volcanic Rocks in Northern Tibet and Their Implications for Crust–Mantle Interaction. Geological Science Press, Beijing, pp. 1–95.
Yin, A., Harrison, T.M., 2000. Geologic evolution of the Himalayan–Tibetan orogen. In: Jeanloz, R., Albee, A.L., Burke, K.C. (Eds.), Annual Reviews of Earth and Planetary Science, vol. 28, pp. 211–280.
Yin, A., Kapp, P.A., Murphy, M.A., Manning, C.E., Harrison, T.M., Grove, M., Ding, L., Deng, X.-G., Wu, C.-M., 1999. Significant late Neogene east–west extension in northern Tibet. Geology 27, 787–790.
Yu, X., 1994. Titanphlogopites from Cenozoic alkaline volcanic rock in western Qinling, Gansu province. Acta Petrologica et Mineralogica 13, 319–327 (in Chinese, with English abstract).
Zhang, H., Harris, N., Parrish, R., Kelley, S., Zhang, L., Rogers, N., Argles, T., King, K., 2004. Causes and consequences of protracted melting of the mid-crust exposed in the North Himalayan antiform. Earth and Planetary Science Letters 228, 195–212.
Zhang, S.Q., Mahoney, J.J., Mo, X.X., Ghazi, A.M., Milani, L., Crawford, A.J., Guo, T.Y., Zhao, Z.D., 2005. Evidence for a widespread Tethyan upper mantle with Indian–Ocean-type isotopic characteristics. Journal of Petrology 46, 829–858.
Zhao, W.L., Morgan, W.J., 1987. Injection of Indian crust into Tibetan lower crust: a two-dimensional finite element model study. Tectonics 6, 489–504.
Zhao, W., Nelson, K.D., Project INDEPTH Team, 1993. Deep seismic reflection evidence for continental underthrusting beneath southern Tibet. Nature 366, 557–559.
Zhao, Z., Mo, X., Zhang, S., Guo, T., Zhou, S., 2000. Geochemistry of the Pliocene shoshonitic rocks from Oiyug basin, central Tibet. Earth Science Frontiers 7 (Suppl.), 107–108.
Zhao, Z., Mo, X., Zhang, S., Guo, T., Zhou, S., Dong, G., Wang, Y., 2001. Post-collisional magmatism in Wuyu basin, central Tibet: evidence for recycling of subducted Tethyan oceanic crust. Science in China (Series D), 44, 27–34.
Zhao, Z., Mo, X., Luo, Z., Zhou, S., Dong, G., Wang, L., Zhang, F., 2003a. Subduction of India beneath Tibet: magmatism evidence. Earth Science Frontiers 10, 149–157 (in Chinese, with English abstract).
Zhao, Z., Mo, X., DePaolo, D.J., Owens, T., Liao, Z., Zhu, D., 2003b. New geochemical data on ultrapotassic rocks in western Tibet. Eos, Transactions — American Geophysical Union 84 (46) Fall Meeting. Suppl., Abstract V32H-02, F1577.
Zhao, Z., Mo, X., Nomade, S., Renne, P.R., Zhou, S., Dong, G., Wang, L., Zhu, D., Liao, Z., 2006. Post-collisional ultrapotassic rocks in the Lhasa Block, the Tibetan Plateau: special and temporal distribution and its implications. Acta Petrologica Sinica 22, 787–794 (in Chinese, with English abstract).
Zhao, Z., Mo, X., Dong, G., Zhou, S., Zhu, D., Liao, Z., Sun, C., 2007. Pb isotopic geochemistry of Tibetan plateau and its implications. Geoscience 21, 269–278 (in Chinese, with English abstract).
Zhao, Z.D., Mo, X.X., Sun, C.G., Zhu, D.C., Niu, Y.L., Dong, G.C., Zhou, S., Dong, X., Liu, Y.S., 2008a. Mantle xenoliths in southern Tibet: geochemistry and constraints for the nature of the mantle. Acta Petrologica Sinica 24, 193–202 (in Chinese, with English abstract).

Zhao, Z., Mo, X., Niu, Y., Zhu, D., Sun, C., Dong, G., Zhou, S., 2008b. Nature of the subcontinental mantle beneath southern Tibet revealed by mantle xenoliths entrained by ultrapotassic rocks. Geochimica et Cosmochimica Acta 72 (Supp.), A1095.

Zhou, H.-W., Murphy, M.A., 2005. Tomographic evidence for wholesale underthrusting of India beneath the entire Tibetan plateau. Journal of Asian Earth Science 25, 445–457.

Zhou, S., Mo, X., Dong, G., Zhao, Z., Qiu, R., Guo, T., Wang, L., 2004. ^{40}Ar–^{39}Ar geochronology of Cenozoic Linzizong volcanic rocks from Linzhou Basin, Tibet, China, and their geological implications. Chinese Science Bulletin 49, 1970–1979.

Zhu, D.C., Pan, G.T., Chun, S.L., Liao, Z.L., Wang, L.Q., Li, G.M., 2008a. SHRIMP zircon age and geochemical constraints on the origin of Early Jurassic volcanic rocks from the Yeba Formation, southern Gangdese in south Tibet. International Geology Review 50, 442–471.

Zhu, D.C., Pan, G.T., Zhao, Z.D., Lee, H.Y., Kang, Z.Q., Liao, Z.L., Wang, L.Q., Li, G.M., Dong, G.C., Liu, B., 2008b. Early Cretaceous subduction-related adakite-like rocks in the Gangdese, south Tibet: products of slab melting and subsequent melt-peridotite interaction? Journal of Asian Earth Sciences 34, 298–309. doi:10.1016/j.jseaes.2008.05.003.

Zhu, D.C., Pan, G.T., Mo, X.X., Wang, L.Q., Liao, Z.L., Zhao, Z.D., Dong, G.C., Zhou, C.Y., 2006. Late Jurassic–Early Cretaceous geodynamic setting in middle-northern Gangdese: new insights from volcanic rocks. Acta Petrologica Sinica 22, 534–546 (in Chinese with English abstract).

Zhou, S., 2002. Study on the geochronology of pivotal regions of Gangdese magmatic and Yarlung Zangbo ophiolite belts, Tibet. Ph. D Dissertation, China University of Geosciences, Beijing (in Chinese, with English abstract).